(A) EPOXY CURING (B) CHARACTERIZATION OF EPOXY/SWNT NANOCOMPOSITES & (C) MnO_2 NANOSTRUCTURES FOR CATALYSIS

By

SATHISH KUMAR LAGESHETTY

Bachelor of Science in Pharmacy
Osmania University
Hyderabad, India
2005

Master of Science in Chemistry
Lamar University
Beaumont, TX
2009

Submitted to the Faculty of the
Graduate College of the
Oklahoma State University
in partial fulfillment of
the requirements for
the Degree of
DOCTOR OF PHILOSOPHY
May, 2015

(A) EPOXY CURING (B) CHARACTERIZATION OF EPOXY/SWNT NANOCOMPOSITES & (C) MnO_2 NANOSTRUCTURES FOR CATALYSIS

Dissertation Approved:

Dr. Kevin D. Ausman

Dissertation Adviser

Dr. Frank D. Blum

Dr. Jeffery L. White

Dr. Richard A. Bunce

Dr. Ranji Vaidyanathan

ACKNOWLEDGEMENTS

I wish to express my sincere gratitude and deepest appreciation to my advisor, Prof. Kevin D. Ausman, for giving me this opportunity to finish this exciting research. Working with Dr. Ausman has been extremely gratifying. I am always thankful to him for giving absolute freedom to work on the problems and approaches of my interest.

I would also like to thank the members of my advisory committee Prof. Frank D. Blum, Prof. Jeffery L. White, Prof. Richard A. Bunce and Prof. Ranji Vaidyanathan for taking time out of their hectic schedules to read my thesis and be on my defense committee. I would also like to thank my collaborators Prof. Frank D. Blum, Prof. Raman Singh, Prof. Richard A. Bunce. Storage modulus and contact angle measurements presented in Chapter IV have been done in Prof. Blum's group by Hamid Mortazavian and Bhishma Sedai respectively. Catalytic activities in Chapter V have been done in Prof. Bunce's group by Dr. Nammalwar. Flexural strength measurements have been done in Prof. Singh's group by Libin Babu.

I am very grateful to my brothers Sandeep and Ajay for their long-standing support. I want to express my gratitude to my son Sriyan. I would also like to deeply thank my beloved wife Sandhya, for being on my side and taking care of me all the time. Last but not least, I wish to dedicate this thesis with love and affection to my parents, Jalaja and Srinivas, and almighty for all the support and encouragement throughout my life.

Name: SATHISH KUMAR LAGESHETTY

Date of Degree: MAY, 2015

Title of Study: (A) EPOXY CURING (B) CHARACTERIZATION OF EPOXY/SWNT NANOCOMPOSITES & (C) MnO2 NANOSTRUCTURES FOR CATALYSIS

Major Field: CHEMISTRY

Abstract: The main objective of this study is to prepare a better material, i.e. stronger, lighter, heat impact and gas permeable for aerospace application. In recent years, the development of filler/epoxy composites has shown large potential for new materials with improved properties. This work was focused on two aspects of epoxy composites: A) the study of cure behavior of sample epoxy amine systems B) the characterization of thermal and mechanical properties of the epoxy nanocomposites. The cure behavior of the sample epoxy amine systems at different concentrations of curing agents and ramp rates were studied by differential scanning calorimetry (DSC). Solvent-dispersed single-walled nanotubes (SWNTs) are incorporated into epoxy matrices, followed by evaporation of the solvent before curing. The effect of solvent choice in thermal and mechanical properties of the resulting nanocomposites is evaluated using N-methyl pyrrolidone and dimethyl formamide. In this study, fluorescence is used as the tool to monitor the dispersions of SWNTs in the solvent and epoxy matrix. This study also compares the thermal and mechanical properties of these epoxy nanocomposites with a nanotube loading ranging from 0.001-0.01 wt. %. Dynamic mechanical analysis results showed increase in the storage modulus of epoxy/SWNT nanocomposites compared to plain epoxy composite. The presence of residual solvent in the epoxy composites is determined by thermogravimetric analysis (TGA). Contact angle measurements showed an increase in the hydrophobicity of the epoxy/SWNT nanocomposites compared to plain epoxy composite.

α-, β-, and γ-MnO_2 were synthesized by hydrothermal methods, and were characterized using x-ray diffraction, scanning electron microscopy, Brunauer Emmett and Teller (BET) surface area, and TGA. TGA analysis showed that α-MnO_2 has greater water content compared to the β- and γ- forms of MnO_2. BET measurements confirmed that the surface areas are in the order of β > α > γ-MnO_2 samples. The catalytic activities of these samples against oxidation of arylmethylene compounds were studied, revealing that the primary factor controlling catalytic activity is the amount of adsorbed water. Additionally, novel structural features of the various forms of MnO_2 will be reported.

.

TABLE OF CONTENTS

Chapter Page

I. INTRODUCTION 1

1.1. Nanomaterials 10
1.2. Polymer composites 11
1.3. Differential Scanning Calorimetry 12
1.4. Polymer Nanocomposites 13
1.5. Nanomaterials for Polymer Nanocomposites 14
1.6. Carbon Nanotubes 15
1.7. Structure of SWNTs 16
1.8. Optical Properties of SWNTs 16
1.9. Absorption Spectroscopy of SWNTs 17
1.10. Fluorescence Spectroscopy of SWNTs 18
1.11. SWNT as Filler Material 18
1.12. Dispersion of SWNTs 19
1.13. Characterization of SWNTs 19
1.14. Nanomaterials in Catalysis 20
1.15. Characterization of MnO_2 21

II. EXPERIMENTAL SECTION 22

2.1. Materials 22
2.2. Preparation of Epoxy/amine composites 23
2.3. Preparation of Epoxy/SWNT Nanocomposite 25
2.4. Sample Preparation for Different Forms of MnO_2 27
2.5. Instrumentation 28

III. Epoxy Curing 36

3.1. Differential Scanning Calorimetry 36

IV. Epoxy/SWNT Nanocomposites 45

4.1. Background 45
4.2. UV/visible-NIR Absorbance Spectroscopy 46

Chapter Page

4.3 Differential Scanning Calorimetry Analysis....47
4.4. Thermogravimetric Analysis....48
4.5. Dynamic Mechanical Analysis....49
4.6. Near Infrared (NIR)-Fluorescence Spectroscopy....51
4.7. Thermogravimetric Analysis....54
4.8. Optical Microscope Images....55
4.9 Dynamic Mechanical Analysis....57
4.10. Contact Angle....58

V. MnO_2 Nanostructures for Catalysis....60

5.1. Brunauer-Emmett-Teller Analysis....60
5.2. Scanning Electron Microscopy Analysis....62
5.3. Thermogravimetric Analysis....63
5.4. Powder X-ray diffraction Analysis....66
5.5. Thermogravimetric Analysis....67
5.6. Brunauer-Emmett-Teller Analysis....68
5.7. Fourier Transform Infrared Spectroscopy....69
5.8. Scanning Electron Microscopy Analysis....69
5.9. Catalytic Activity....71

V. Conclusions....73

REFERENCES....75

APPENDICES....78

LIST OF TABLES

Table Page

Table 2.1. Properties of EPON 828 23
Table 2.2. Amount of epoxy resin and amines for cure behavior.....24
Table 2.3. Properties of EPON 862 25
Table 3.1. Curing characteristics of Epon 828/IPDA and Epon/DMD systems.....37
Table 5.1. BET surface areas of commercial MnO_2, Attenburrow MnO_2 and nano-MnO_2 61
Table 5.2. Oxidation of diphenylmethane to benzophenone using three different forms of MnO_2 samples.....61
Table 5.3. BET surface area of α-, β-, and γ-MnO_2 nanostructures.....68
Table 5.4. Oxidation of diphenylmethane to benzophenone using α-, β-, γ-MnO_2 samples dried at two different temperature 71

LIST OF FIGURES

Figure Page

1.1 Chemical structures of (a) Oligomeric form of DGEBA, where n = 0 to 25 (b) Oligomeric form of DGEBF, where n = 0 to 25 11
1.2. Typical DSC thermogram for curing epoxy system 13
1.3. van Hove singularities of (a) metallic (b) semiconducting SWNTs 17
2.1. Chemical structures of (a) Oligomeric form of DGEBA, where n = 0 to 25 (b) IPDA and (c) DMD 24
2.2. Chemical structures of (a) Oligomeric form of DGEBF, where n = 0 to 25 and (b) AMICURE PACM 26
2.3. Schematic of the sample preparation of Epoxy/SWNT nanocomposites 27
2.4. Schematic of the sample polishing tool for epoxy/SWNT nanocomposites.....30
2.5. Schematic of the polishing instrument (a) before and (b) after installation of tool 31
2.6. Three point bend test of epoxy nanocomposite at span length of 65mm.....33
3.1. DSC curves of Epon 828/IPDA and Epon 828/DMD systems at 10 °C/min heating rate.....37
3.2. DSC curves of (a) Epon 828/IPDA and (b) Epon 828/DMD systems at different heating rates.....38
3.3. T_g curves of Epon 828/IPDA at different heating rates (10,5, 1 °C/min).....39
3.4. DSC curves of (a) Epon 828/IPDA and (b) Epon 828/DMD systems for various amounts of curing agents at 10 °C/min.....40
3.5. T_g curves Epon 828/IPDA cured at various amounts of curing agents at 10 °C/min.....42
3.6. DSC thermograms of Epon 828 cured with Cyclohexylamine and Dicyclohexylamine at 1 °C/min heating rate 43
4.1. Comparison of the SWNTs dispersed in NMP (a) before centrifugation (b) after centrifugation 47
4.2. Variation of glass transition (T_g) temperature with amount of filler loading 48
4.3. TGA of neat resin and epoxy/SWNT nanocomposites (a) in air (b) in nitrogen.....49
4.4. Variation of storage modulus with amount of filler loading (0.001-0.01 wt.%) 50
4.5. SWNT fluorescence taken at 658 nm excitation while dispersed in NMP (black) and DMF (red) 51

Figure Page

4.6. SWNT fluorescence taken at 658 nm excitation with addition of Epon-862 to NMP (black) and DMF (red) dispersions 52
4.7. SWNT fluorescence taken at 658 nm excitation without addition (black) and with addition of Epon-862 to NMP dispersions 53
4.8. TGA analysis of SWNT/epoxy composite at different loadings ranging from 0.001 wt%-0.01 wt% 54
4.9. Optical microscope images of SWNTs dispersed in the epoxy nanocomposites 56
4.10. Storage modulus of epoxy nanocomposites at various loadings (0.001-0.01wt. %) of SWNTs 58
4.11. Contact Angle of epoxy nanocomposites at various loadings (0.001-0.01wt.%) of SWNTs 59
5.1. SEM images of the (a) Nano-MnO_2 (b) Attenburrow MnO_2 and (c) commercial MnO_2 62
5.2. TGA curves of MnO_2 samples 64
5.3. Correlation of MnO_2 surface water content with reactivity 65
5.4. Powder x-ray diffraction (XRD) pattern of the as-prepared α-, β-, γ-MnO_2 samples 66
5.5. TGA results for different crystalline forms of MnO_2 samples 67
5.6. FTIR spectra of the as-prepared α-, β-, γ-MnO_2 samples 69
5.7. SEM images of the as-prepared (a) α- (b) β- and (c) γ-MnO_2 samples 70

CHAPTER I

INTRODUCTION

1.1. Nanomaterials

Nanomaterials are materials in which at least one of the dimensions is in the nanometer range (≤ 100 nm).[1] Typical nanomaterials include nanoparticles, nanotubes, nanofibres, fullerenes, and nanowires. In general, these materials are classified into three classes such as particle (silica, metals), layered (graphite, layered minerals) and fibrous (nanotubes).[2,3] Reduction of particle size to nanometer size can modify the physical and chemical properties of nanomaterials, often improving the properties of bulk counterparts. In this study we used nanomaterials in two different systems. In the first case, nanomaterials were used as smaller stronger fillers in a composites, and when dispersed homogeneously showed improvement in the bulk properties of the prepared nanocomposites. In the second case, nanomaterials were used in a catalytic system, where the increase in the surface area has potential to show improvements in catalytic activity.

1.2. Polymer composites

Epoxy resins are the most widely used polymer matrices for composites. Epoxy resins are polymers which contain more than one unreacted oxirane group. These are mainly classified into two types: diglycidyl ether of bisphenol-A (DGEBA) and diglycidyl ether of bisphenol-F (DGEBF).

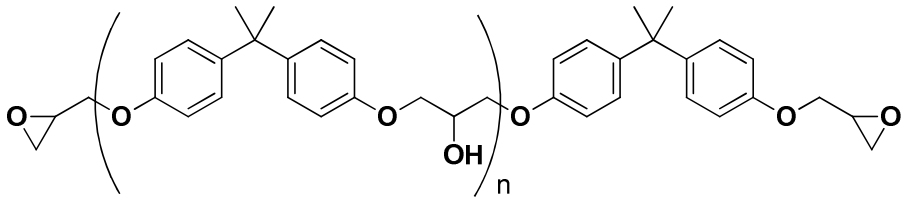

a

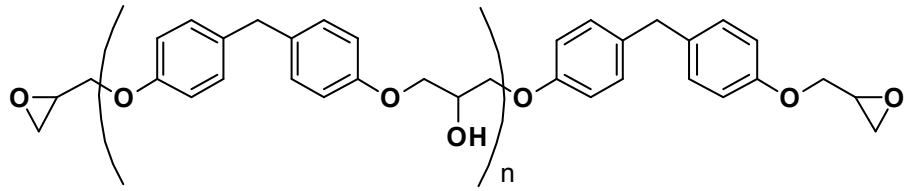

b

Figure 1.1. Chemical structures of (a) oligomeric form of DGEBA, where n = 0 to 25 (b) oligomeric form of DGEBF, where n = 0 to 25.

DGEBA is usually synthesized by the reaction of bisphenol-A with epichlorohydrin. Due to their heat resistance and excellent adhesion properties these are widely used in various applications that include protective coatings, aerospace industry and adhesives. In general, the applications of this matrix are limited due to its poor thermal conductivity and

brittle nature. The two important approaches to overcome these limitations include: (a) optimization of cure conditions and (b) incorporation of filler materials.

As mentioned earlier, due to its high thermal stability and physical properties, we selected epoxy resin as our matrix to improve the properties. Curing is the process in which a three-dimensional crosslinked network is formed from a chemical reaction of an epoxy resin with a curing agent (hardener). The curing agent mainly transforms the liquid epoxy resin into a solid composite. The curing process proceeds by opening the epoxide group through reaction with the amine of the curing agent. The final properties of the crosslinked network depend upon the type of epoxy, structure of the curing agent and curing conditions.[4,5] Hence optimization of curing conditions, such as amounts of curing agent, temperatures will be helpful in improving the properties of the epoxy composite. In this study, we have used differential scanning calorimetry as technique to understand the curing behavior for optimization of curing processes.

1.3. Differential scanning calorimetry

Differential scanning calorimetry (DSC) is a thermal analysis technique that measures heat flow as a function of temperature at specific ramp rate. DSC is a widely used technique to understand the curing process. The extent of cure in DSC is mainly determined by measuring the heat of the reaction. This technique provides excellent information about the onset of cure, completion of cure, heat of cure and glass transition temperature (T_g). Figure 1.2 shows a typical trace for curing an epoxy system.

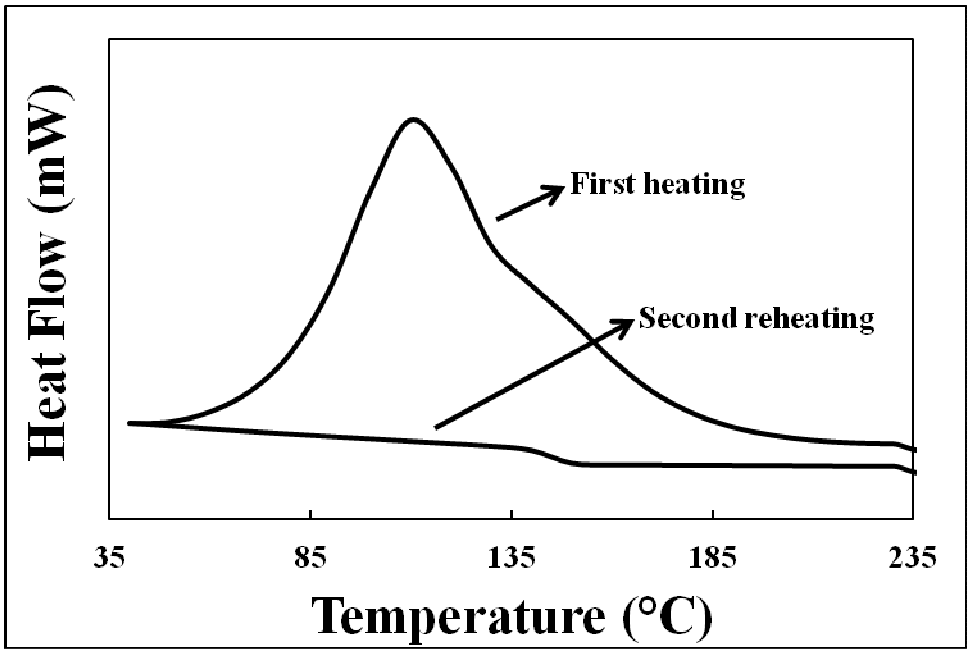

Figure 1.2. Typical DSC thermogram for curing epoxy system.

Consistent with the above figure, the first cycle of heating gives information about curing. The heat of the curing reaction can be obtained by integrating the area under the exothermic peak. After cooling, the second reheating gives information about the glass transition temperature (T_g). The glass transition temperature will correlate with properties such as modulus and tensile strength. The linear behavior in the second reheating at the curing regime of first heating indicates the completion of cure. If the curing is incomplete, an exothermic peak may be observed in second heating cycle.

1.4. Polymer nanocomposites

The term "nanocomposite" was first used by Roy (1993) and Komarneni (1992). Nanocomposites are the materials that are made from two or more distinct phases to achieve better properties in a single component. These materials are usually a blend of

nanocomponents (≤ 100 nm) in at least one of the dimensions, which act as a reinforcing material dispersed in the polymer matrices.

There are several polymer matrices that are reported in the literature.[6] These include polyolefins such as polypropylene,[7,8] polyethylene;[9,10] vinyl polymers such as polystyrene,[11,12] polyacrylamide,[13] polymethyl methacrylate;[14,15] several others such as polyurethanes,[16,17] polyamides[18,19] and epoxy polymer resins.[20-22]

The two different approaches for the preparation of nanocomposites include bottom-up and top-down methods. The bottom-up approach includes synthesis of nanoparticles along with polymers using precursors via a sol-gel process. The top-down approach includes dispersing nanoparticles into a polymer matrix. In this study we followed the latter approach as described in the experimental section.

The uniform improvement in composite properties typically depends heavily on the quality of filler dispersion within the matrix. Nanomaterials or nanofiller, due to their exceptional large surface areas, are expected to show dramatic improvement in the final properties of the polymer nanocomposites. However, dispersion of these nanomaterials is not easily achieved because of strong van der Waals forces that result in agglomerations.

1.5. Nanomaterials for polymer nanocomposites

A wide variety of materials have been investigated as nanomaterials in the recent literature. Due to their high aspect ratios, nanomaterials provide high efficiency as filler

materials.[23] The nanomaterials are mainly classified into three types based on their geometries.[24]

Nanoclays (such as layered silicates) and exfoliated graphite are some of the examples of layered nanomaterials. These nanomaterials are extensively studied to improve the bulk properties of the nanocomposites.[25-27]

Silica, TiO_2 nanoparticles, metals, and polyhedral oligomeric silsesqiuoxanes (POSS) are some of the most common examples for particles used reinforcing nanocomposites. These nanomaterials are widely investigated to improve thermal, mechanical and barrier properties.[28-31]

Carbon nanotubes, cellulose whiskers and nanofibres are some of the examples of fibrous nanomaterials. These nanomaterials offer advantages over layered and nanoparticles due to their high aspect ratios. Single-walled carbon nanotubes (SWNT) being the toughest material (tensile strength of 30 GPa and Young's modulus of 1000 GPa)[32] are the most-studied nanomaterials for polymer nanocomposites.

1.6. Carbon nanotubes (CNTs)

Carbon nanotubes are the fourth discovered allotrope of carbon, first discovered by Ijima in 1991.[33] Since then, carbon nanotubes have attracted considerable interest as materials for a variety of applications including electron field emitters, lithium and hydrogen storage, nanocomposites etc.[34] The diameters of carbon nanotubes range from 0.5-3 nm. Due to the small diameters, these materials are extremely strong and quite stiff (meaning high

tensile strength and high Young's modulus).[32] CNTs are mainly classified into two structural forms: Single-walled carbon nanotubes (SWNTs), with one layer of graphene wrapped into a seamless cylinder and multi-walled carbon nanotubes (MWNTs), with multiple layers of graphene. Production of large quantities of SWNTs is very difficult compared to MWNTs. Synthesis of SWNTs involves various methods, such as electric arc discharge,[35,36] chemical vapor deposition,[37,38] laser ablation,[39] and CoMocat method.[40,41] In the present work, I will be focusing on SWNTs.

1.7. Structure of SWNTs

SWNTs may be either metallic or semiconducting, depending upon the axis along which the graphene sheet is rolled up to form the nanotube. The structures of the SWNTs are expressed by a chiral vector (C_h). This gives the relative location of the two sites on the graphene sheet upon rolling. The diameter of nanotube and direction in the graphene sheet plain can be obtained by two pair of integers (*n, m*), which specify the chiral vector. The angle between chiral vector and the nearest unit vector is defined as the chiral angle (θ).[42] Based on chiral angles and chiral vectors, SWNTs are either of the arm chair ($n = m$), zigzag ($n = 0$ or $m = 0$) or chiral (any other n or m).

The electronic properties of the SWNTs are determined based on the (*n, m*) designation. All arm chairs ($n = m$) are metallic with the finite density of states at the fermi energy level. Others with $n\text{-}m = 3k$, where k is a nonzero integer, are semiconductors with a band gap.

1.8. Optical properties of SWNTs

The quasi-one-dimensionality of the semiconducting SWNTs causes the electron state densities to have characteristic van Hove peaks.[43,44] Energies between the van Hove singularities differ with nanotube structure. The electronic transitions between the van Hove singularities are produced by the optical absorption of a specific nanotube. These electronic transitions will result in unique optical properties of SWNTs. Figure 1.3 shows the schematic of density of electron states diagram for metallic and semiconducting SWNT, showing van Hove singularities.

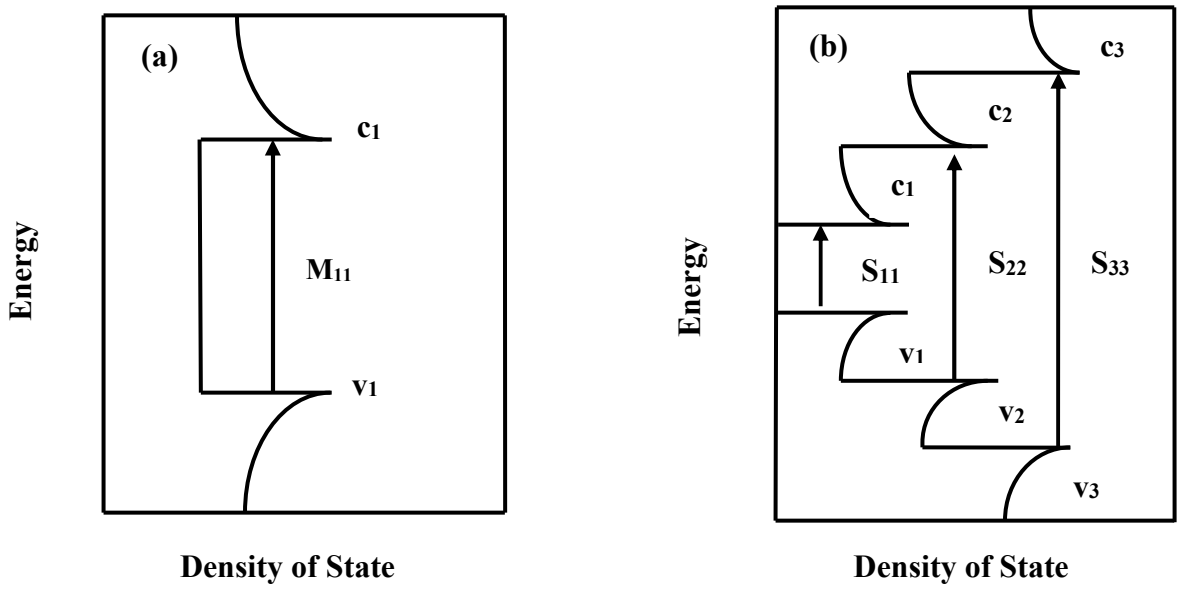

Figure 1.3. van Hove singularities of (a) metallic (b) semiconducting SWNTs.

1.9. Absorption spectroscopy of SWNTs

Optical absorption of SWNTs originates from valence sub band (v_1, v_2, v_3) to the corresponding conduction sub bands (c_1, c_2, c_3). The optical transition from c_1 to v_1 is identified as a metallic interband transition (M_{11}), while the transition from c_2 to v_2 to and c_3 to v_3 are identified as semiconducting interband transitions (S_{11} and S_{22}). The values of these interbrand transitions will range from 0.5 to 4 eV, based on the chiral vectors of SWNTs.

1.10. Fluorescence spectroscopy of SWNTs

The recent discovery of band gap fluorescence from semiconducting SWNTs in aqueous surfactant suspensions opened the door for quantitative determination of detailed tube structures.[43] Band gap fluorescence is observed only by semiconducting SWNTs. When an electron is excited from v_2 to c_2 by absorbing energy, it creates a hole in valence band v_2. The rapid relaxation of hole and electron will take place, followed by electron hole recombination through the first van Hove transition via fluorescence emission in the near-infrared region. In metallic SWNTs the continuous density of states through fermi levels allows a nonradiative pathway. The electron transfer from a metallic tube to adjacent semiconducting SWNTs will quench the fluorescence. Therefore a SWNT bundle does not exhibit fluorescence. Approximately one third of SWNTs in any sample are metallic. Fluorescence is only observed in sample which contains individual semiconducting SWNTs.

1.11. SWNTs as filler material

In recent years, SWNTs have shown great potential as promising filler materials for numerous applications. However, the practical application of this material is limited due to factors such as aggregation of the SWNTs, and poor load transfer between polymer matrices and SWNTs. [45-47]SWNTs, as synthesized, exist in highly aggregated forms due to strong van der Waals forces. In order to take advantage of superior properties of SWNTs, these should be well dispersed in individual form into the polymer matrices.

1.12. Dispersion of SWNTs

There are several methods reported in the literature that tried to improve dispersion of the SWNTs. These include covalent functionalization of SWNT end-caps with aliphatic amines[48] and side-walls with fluorine.[49,50] However, improved dispersion of SWNTs in solvents and polymer matrices by chemical modification is considered as a destructive approach because the mechanical and electronic properties of the SWNTs are affected by the disruption of π electrons in the system. Ultrasonication dispersed SWNTs in water with the aid of surfactants[51] was effective in dispersing SWNTs, but removing the surfactant afterwards was problematic. Ultrasonication by itself was a good technique, but the cavitation bubbles that are active in dispersion collapse at high temperatures and pressure induce damage to the nanotubes.[52] Therefore, careful optimization of ultrasonication to maximize dispersion and minimizing the nanotubes is desired for achieving the improved properties of nanocomposites. In this work, I will be discussing the individualization of

SWNTs observed by careful optimization of ultrasonication in both the solvent and epoxy matrix.

1.13. Characterization of SWNTs

Traditional nanocharacterization techniques are vital for any nanomaterials work. However, for nanocomposites no information is more important than the quality of dispersion in both the solvent and epoxy matrices. Herein, we report a novel application of fluorescence as a probe to monitor individualization of carbon nanotubes. This technique surpasses all microscopy techniques, particularly against a carbonaceous background.

1.14. Nanomaterials in catalysis

The main motivation for this work was from Dr. Bunce's group to find an efficient catalyst for oxidation of arylmethylene compounds. Earlier methods used chromium based reagents[53] for benzylic oxidations, which were messy and produce environmentally hazardous wastes. Other catalysts available in the literature used for this purpose were MnO_2, but these materials suffered a drawback of using large quantities. Therefore, a smaller size nanomaterial that imparted maximum surface area to the reactant, allowed greater reactivity and increased the yield. In this search, they found a nano surface catalyst nano-MnO_2 which showed a higher catalytic activity compared to Attenburrow MnO_2 and commercial MnO_2.

This part of work was mainly focused on the characterization of nano-MnO_2 to elucidate the reason for its higher catalytic activity. The results suggested that adsorbed water

correlated with the activity of the catalyst.[54] To further probe the reasons for the catalytic activity of MnO_2, we synthesized three different crystalline forms of MnO_2.

Manganese dioxide (MnO_2) primarily exists in three crystallographic forms α-, β-, and γ-MnO_2. In all the three cases, the main structural unit is MnO_6 octahedra, but connected differently.[55] These materials have some properties that differ among crystallographic forms, and the similarities outweigh the differences. MnO_2 with various physical and chemical properties such as crystallographic form, surface area and water content can be synthesized under different conditions. Earlier many methods for the preparation of manganese oxide materials were used including a sol-process, microwave heating, and precipitation/ion-exchange.[56] While numerous methods have been used to prepare MnO_2 with various structures[57,58] hydrothermal methods are the most commonly employed. Because of various crystallographic forms, MnO_2 has applications in catalysis, ion-sieves, cathode materials for rechargeable batteries, and super capacitors.[59-62]

In the present study, we synthesized and characterized different polymorphs in order to determine whether the previously reported adsorbed water content was the only significant factor in determining the catalytic activity.

1.15. Characterization of MnO_2

To understand in detail the significance of the crystallinity, water content and surface area, characterization of MnO_2 was performed. The characterization techniques performed to determine these parameters included X-ray diffraction, thermogravimetric analysis, scanning electron microscopy and BET surface area analysis. The prepared catalysts were evaluated based on their ability to accomplish oxidation of diphenylmethane to benzophenone.

CHAPTER II

EXPERIMENTAL SECTION

2.1. Materials

Purified CoMoCAT CG300 single walled carbon nanotubes were obtained from Southwest Nanotechnologies, Inc. EPON 828 and EPON 862 resins were obtained from MOMENTIVE, Inc. Amicure PACM was obtained from Air Products and Chemicals, Inc. Isophorone diamine (IPDA) was obtained from Momentive. 4, 4'-Methylenebis(2-methylcyclohexylamine) **(**DMD) was obtained from Aldrich. 1-Methyl-2-pyrrolidinone (NMP) and dimethylformamide (DMF) were obtained from Sigma-Aldrich and used as received. Manganese sulfate was obtained from Mallinckrodt, Inc. Ammonium per sulfate, ammonium sulfate and potassium chlorate were obtained from Sigma-Aldrich.

2.2. Preparation of epoxy/amine composites

2.2.1. Selection of epoxy resin, curing agent

A diglycidyl ether of bisphenol A type, EPON resin 828 was used as the epoxy resin. This resin is an undiluted, clear, difunctional epoxy resin produced from bisphenol A and epichlorohydrin. EPON 828 was specially developed to provide very good mechanical properties, dielectric and chemical resistance. The properties of EPON 828 resin are listed below in Table 2.1.

Properties	Units	Value
Weight per Epoxide	g/eq	185-192
Viscosity at 25 °C	P	110-150
Density	lb/gal	9.7

*Source-Technical Data Sheet of EPON 828

Table 2.1. Properties of EPON 828*

The curing agents used were cycloaliphatic amines, isophorone diamine (IPDA) with a molecular weight of 170.30 g and 4, 4'-methylenebis(2-methylcyclohexylamine) (DMD) with molecular weight of 238.41 g. The structures of the epoxy resin and curing agent are shown in Figure 2.1.

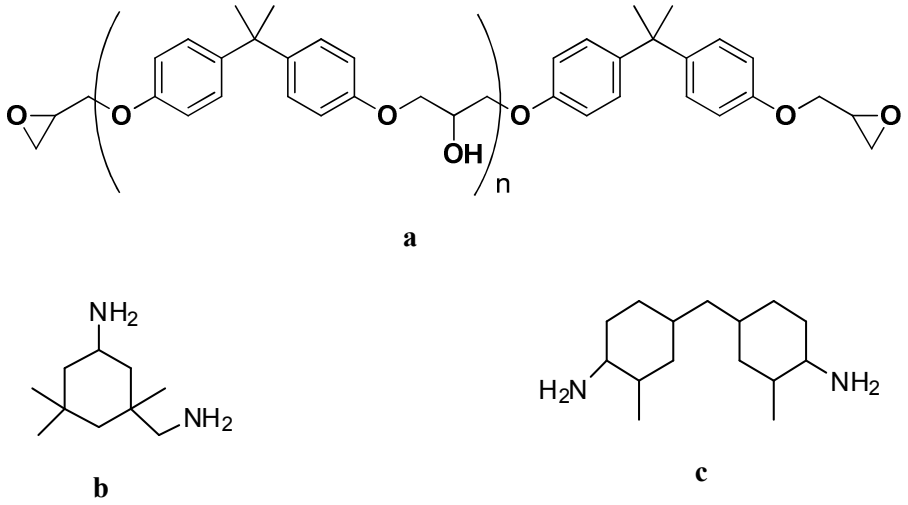

Figure 2.1. Chemical structures of (a) oligomeric form of DGEBA, where n = 0 to 25 (b) IPDA and (c) DMD

2.2.2. Sample preparation for cure behavior of epoxy-amine

DGEBA epoxy type Epon-828 and curing agents IPDA, DMD were mixed at multiple ratios at room temperature. The amounts of epoxy and amines employed are listed in Table 2.2. The resultant materials were completely mixed by a mechanical overhead stirrer and degassed with a vacuum pump to eliminate the air bubbles.

Epon-828 (g)	IPDA (g)	DMD (g)
100	30	-
100	22.4	-
100	12	-
100	6	-
100	-	31.3
100	-	15

Table 2.2. Amount of epoxy resin and amines for cure behavior

2.3. Preparation of epoxy/SWNT nanocomposites

2.3.1. Selection of epoxy resin, curing agent

A diglycidyl ether of bisphenol F type, EPON resin 862 was used as the epoxy resin. This resin is a low viscosity, undiluted difunctional epoxy resin produced from bisphenol F and epichlorohydrin. EPON 862 was specially developed to provide very good mechanical properties, adhesive, chemical resistance and ease of fabrication. Preparation of epoxy/SWNT nanocomposites requires a low viscosity epoxy resin to overcome processing difficulties.[63] The properties of EPON 862 resin are listed in Table 2.3.

Properties	Units	Value
Weight per Epoxide	g/eq	165-173
Viscosity at 25 °C	P	25-45
Density	lb/gal	9.8

*Source-Technical Data Sheet of EPON 862

Table 2.3. Properties of EPON 862*

The curing agent used was cycloaliphatic diamine, AMICURE PACM with a molecular weight of 210.36 g. The structures of the epoxy resin and curing agent are shown in Figure 2.2.

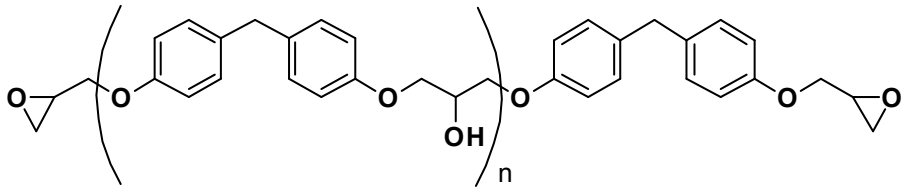

a

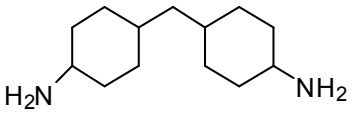

b

Figure 2.2. Chemical structures of (a) oligomeric form of DGEBF, where n = 0 to 25 and (b) AMICURE PACM

2.3.2. Sample preparation for epoxy/SWNT nanocomposites

SWNT/epoxy nanocomposites were prepared with nanotube loadings of 0.001, 0.005 and 0.01 wt. %. The purified nanotubes were dispersed in *N*-methylpyrrolidone (NMP) or N, N-dimethylformamide (DMF) solvents by bath sonication for 24 h. The epoxy resin, Epon-862 was then mixed with the nanotube dispersion in the solvents and sonicated for 1 h. Both solvents, NMP and DMF, were evaporated at 150 °C and 165 °C respectively, under vacuum for 4 h. The resulting mixture was cooled to room temperature and degassed for 30 min. The curing agent (resin:curing agent = 3:1) was added, mixed using an overhead stirrer for 30 min, degassed again to remove any air bubbles and then poured into molds and pre-cured at 80 °C for 2 h and post-cured at 150 °C for 2 h. Figure 2.3 shows a schematic of the method for the preparation of epoxy nanocomposites.

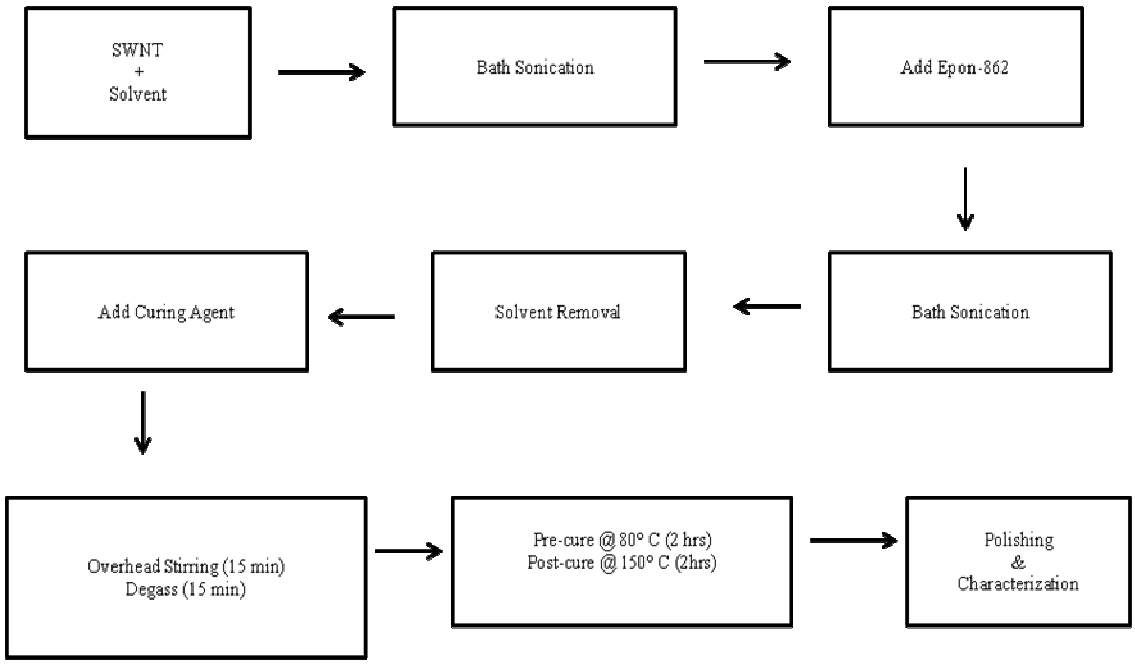

Figure 2.3. Schematic of the sample preparation of epoxy/SWNT nanocomposites

2.4. Sample Preparation for Different Forms of MnO_2

All reagents were analytical grade and used as received without further purification. In a typical synthesis of β-MnO_2, 1.35 g of manganese sulfate and 1.83 g of ammonium persulfate powders were mixed in 70 mL of deionized water until a clear solution was formed and then transferred into a Teflon-lined stainless steel autoclave, sealed and heated in an oven at 120 °C for 12 h. After the reaction was completed, the resulting black solid was filtered, washed with deionized water and dried in an oven at 90 °C and 120 °C. The preparation of α-MnO_2 followed an identical process, except with 1.98 g of ammonium sulfate was added to the reaction system.[64] The γ-MnO_2 synthesis also followed the same process, but with 1.00 g of manganese sulfate and 1.50 g of potassium chlorate mixed in 70 mL of deionized water, and heated in an oven at 160 °C for 18 h. followed by filtration and drying at 90 °C and 120 °C.[65]

2.5. Instrumentation

2.5.1. Ultrasonication and Centrifugation

A FS-140H ultrasonic bath using 135 W of power was used to disperse SWNTs in both the solvent (8 h) and epoxy matrix (1 h). A Sorvall Biofuge Stratos centrifuge was used to separate individual SWNTs from bundles using low speed centrifugation at a speed of 1500 rpm for 2 h.

2.5.2. Absorption Spectroscopy

A Varian Cary-5000 spectrophotometer was used to monitor the dispersion of SWNTs in the solvent before and after centrifugation. The UV/Vis-NIR measurements of SWNTs dispersed in the solvents were carried out in 1 mm path-length quartz cells. The absorption spectra showed distinct peaks of SWNTs in the range of 400 to 1600 nm.

2.5.3. NIR-Fluorescence Spectroscopy

An Applied Nanofluorescence NS-1 Nanospectralizer was used to acquire near-infrared-fluorescence spectra of the SWNTs dispersed in both solvent and epoxy matrix using 658 and 782 nm excitation lasers.

2.5.4. Differential Scanning Calorimetry (DSC)

A TA instrument DSC Q2000 was used to determine the changes in the glass transition temperature due to dispersion of SWNTs into epoxy matrix. The samples (5-10 mg) were heated from room temperature to 250 °C at a ramp rate of 10 °C/min, maintained at 250 °C for 0.5 min, then cooled to 25 °C at ramp rate of 10 °C, held at 25

°C for 0.5 min., and finally heated again to 250 °C at a ramp rate of 10 °C/min, all under a nitrogen atmosphere. Indium was used as a calibration standard. The first heating ramp monitored the curing process, while the second heating ramp determined the glass transition temperature of the fully-cured sample.

The curing behavior of the sample epoxy amine samples was similarly obtained at ramp rates of 0.5, 1, 3, 5 and 10 °C/min. The exothermic heat flow was determined from the first heating and the glass transition was obtained from the second heating.[66]

2.5.5. Thermogravimetric Analysis (TGA)

A Mettler Toledo TGA/SDTA851e instrument was used to evaluate the epoxy nanocomposite samples for residual solvent and thermal decomposition. The samples (5-10 mg) were heated from 30.0 to 800 °C at a ramp rate of 10.0 °C/min under nitrogen atmosphere at a flow rate of 20 mL/min.

A Mettler Toledo TGA/DSC STAR e system was used to determine the structural water content of the synthesized α-, β-, and γ-MnO_2 nanomaterials. The samples were heated from 30.0 to 500 °C at a ramp rate of 10.0 °C/min.

2.5.6. Polishing Sample Surfaces

An Inland Swap Top Flat Lap polishing machine was used to polish the prepared epoxy nanocomposites. Figure 2.4 shows a schematic of the tool developed for polishing sample surfaces. The tool consists of four parts (a) a main holder (b) an aluminum metal surface with teflon lining (c) an aluminum metal surface without teflon lining (d) a brass metal support.

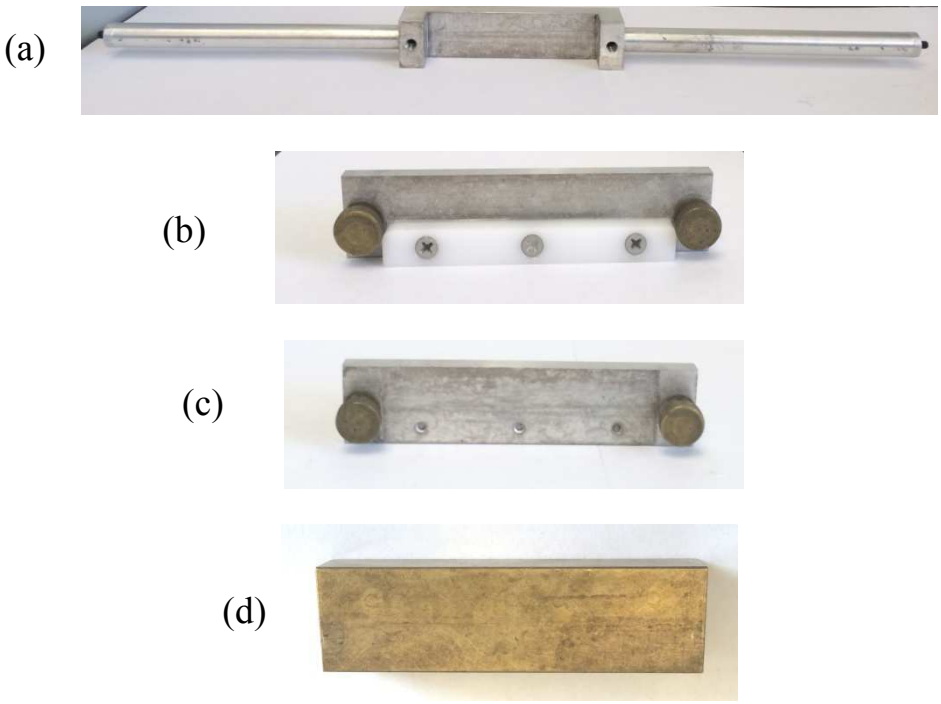

Figure 2.4. Schematic of the sample polishing tool for epoxy/SWNT nanocomposites.

The main holder and aluminum metal with teflon lining are attached to polish the top and bottom surface of the epoxy nanocomposites. The brass metal is used to apply some force on the sample while polishing. The main holder and aluminum metal without teflon lining are attached to polish the remaining surfaces of the sample. Figure 2.5 shows the schematic of the polishing instrument before and after installation of the tool.

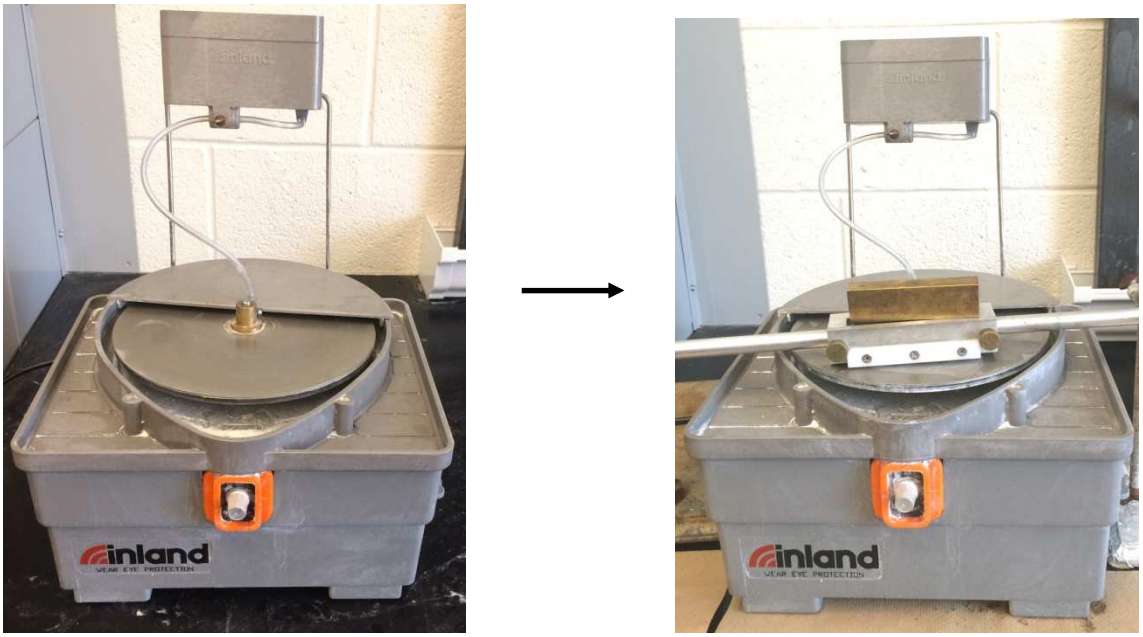

(a) (b)

Figure 2.5. Schematic of the polishing instrument (a) before and (b) after installation of tool.

2.5.7. Dynamic mechanical analysis (DMA)

A TA instrument DMA Q800 was used to determine the storage modulus (E′), loss modulus (E″) and tan delta of prepared epoxy nanocomposites. Three point bending test were carried out with a sample sizes of 35 x 15 x 5 mm by heating the samples from room temperature to 250 °C at a ramp rate of 5 °C/min by applying a constant sinusoidal displacement of 20 μm with a frequency of 1 Hz. For each sample group, three replicates were tested.

2.5.8. Fracture toughness measurement

An Instron 5567, universal testing machine was used to determine the fracture toughness of the epoxy/SWNT nanocomposites. Fracture toughness was determined using a single edge notch bend test as per the ASTMD-5045 standard method. A 4.5 mm deep notch was cut using a diamond precision saw in each of the 54 x 12.7 x 6.35 mm samples prepared. The tip of the notch was tapped with fresh razor blade using a hammer, to initiate a natural pre-crack. The pre-crack single edge notch specimen was loaded under three point bending test until failure. A minimum of 3 samples were tested for each type of nanocomposite. The fracture toughness of the epoxy/SWNT nanocomposites was expressed in term of critical stress intensity factor (K_{IC}) according to following equation:

$$K_{IC} = \frac{P}{B\sqrt{W}} f\left(\frac{a}{W}\right)$$

where P is the maximum applied force, B is the thickness of the specimen, W is width of the specimen and f is the geometric factor calculated by following equation:

$$f\left(\frac{a}{W}\right) = \frac{3\frac{S}{W}\sqrt{\frac{a}{W}}}{2\left(1+2\frac{a}{W}\right)\left(1-\frac{a}{W}\right)^{1.5}} \times \left[1.99 - \left(\frac{a}{W}\right)\left(1-\left(\frac{a}{W}\right)\right)\left(2.15 - 3.93\frac{a}{W} + 2.7\left(\frac{a}{W}\right)^2\right)\right]$$

2.5.9. Flexural strength

An Instron 5567, universal testing machine was used to determine the flexural modulus and strength of the epoxy/SWNT nanocomposites. Flexural modulus was determined using a three point bend test as per the ASTMD 790 standard method. The

specimen was loaded under three point bending test until failure. Figure 2.6 shows an epoxy nanocomposite specimen in a three point bend test.

Figure 2.6. Three point bend test of epoxy nanocomposite at span length of 65mm.

Sample analysis was performed at a fixed cross head speed which is calculated by following equation:

$$R = \frac{ZL^2}{6d}$$

where Z = 0.01, L is the span length and d is the thickness. The flexural strength of the epoxy/SWNT nanocomposites was calculated by:

$$\sigma_f = \frac{3PL}{2bd^2}$$

where P is the maximum load bear by the specimen, L is the span length, b is the width and d is the thickness.

2.5.10. Optical microscope

An inverted Olympus IX83 microscope was used to coarsely evaluate the agglomeration behavior of SWNTs in the cured epoxy nanocomposites. Optical images of the SWNTs dispersed initially in NMP and DMF solvents in the cured epoxy nanocomposites was taken at a magnification of 20x for loadings ranging from 0.001 wt.% -0.01 wt.% .

2.5.11. X-ray powder diffraction

A Bruker D8-advance X-ray diffractometer with Cu Kα radiation (λ = 1.5406 Å) was used to determine the powder X-ray diffraction (XRD) patterns of the prepared α-,β-, and γ-MnO_2 samples. The data were collected at an operating voltage of 40 kV and the current was maintained at 40 mA.

2.5.12. Scanning electron microscopy

An FEI Quanta 600 field emission scanning electron microscope equipped with an Evex EDS X-ray analysis system was used to evaluate the fractured surfaces of the epoxy/SWNT nanocomposites, and the size and morphology of the prepared α-,β-, and γ-

MnO_2 samples. The SEM images of the samples were taken at an acceleration voltage of 20 kV.

The fracture surfaces of the epoxy/SWNT nanocomposites were sputter-coated with gold using a magnetron sputter coater. Sputtering was performed in vacuum, maintaining a pressure between 8 and 2 x 10^{-2} mbar. Gold was deposited on the sample at the rate of 25 nm/min at a sputtering voltage 3 kV. The gold-coated sample was then mounted on the SEM stage to collect micrographs.

2.5.13. Surface area

A Quanta Chrome instrument was used to determine the Brunauer-Emmet-Teller (BET) surface areas of the samples using N_2 adsorption with the multipoint method. BET is the most widely used technique to calculate the surface area of MnO_2 samples. The adsorbate used for the BET surface area determination is nitrogen at 77 K. The amount adsorbed (V), is measured as a function of relative pressure (p/p_o), where p_o is the saturation vapor pressure. Before analysis, samples are degassed under vacuum overnight, to remove the trapped moisture.[67]

2.5.14. Fourier transform infrared (FTIR) spectroscopy

A Perkin Elmer system 2000 FTIR was used to determine the chemical composition of the prepared α-, β-, and γ-MnO_2 samples. FTIR analysis was performed from 4000 to 400 cm^{-1} using 64 scans at a resolution of 4 cm^{-1}. Samples were finely powdered and pressed into KBr pellets before collecting the spectra.

CHAPTER III

EPOXY CURING

The main objective in this study was to understand the curing behavior for the systems we will be studying in the next project, relating to SWNT composites, and try to optimize the conditions for curing. As mentioned earlier, DSC is a widely-used technique to monitor the curing behavior of epoxy systems.

3.1. Differential scanning calorimetry (DSC)

Figure 3.1 shows typical DSC thermograms of the DGEBA-type epoxy, Epon 828, cured with IPDA and DMD. The DSC thermograms of the two systems Epon 828/IPDA and Epon/DMD in the figure below provides excellent information about the onset temperature, peak temperature, final temperature and exothermic heat.

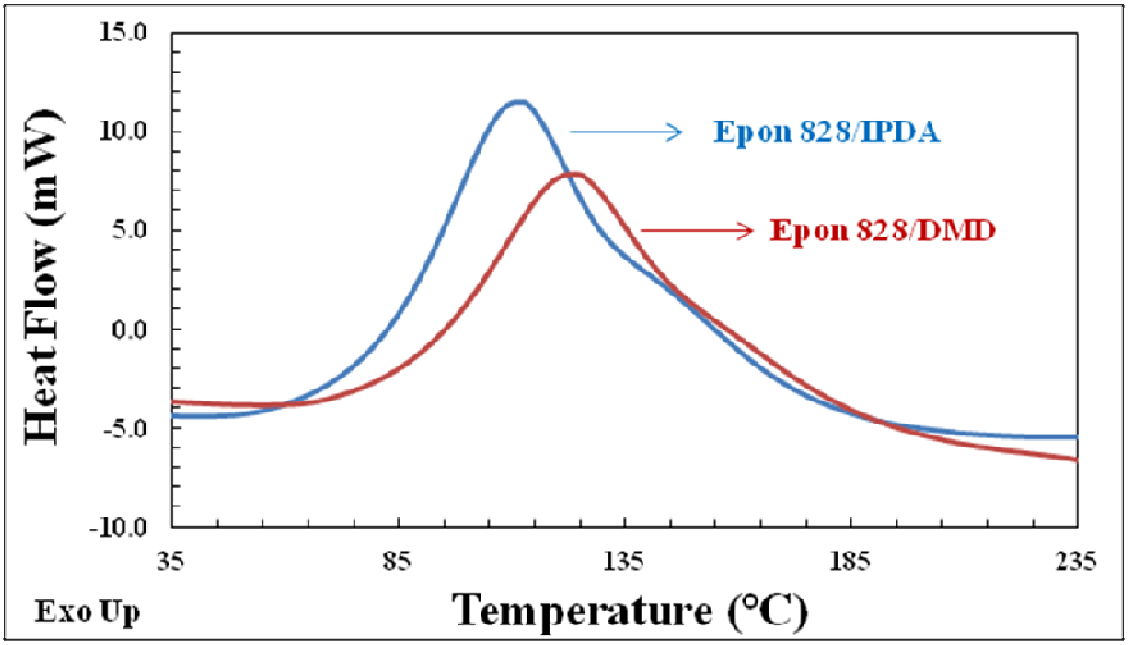

Figure 3.7. DSC curves for Epon 828/IPDA and Epon 828/DMD systems at 10 °C/min heating rate.

The obtained data from this curing reactions are listed in Table 3.1.

Samples	**T_i (°C)**	**T_p (°C)**	**T_f (°C)**	**ΔH (J g^{-1})**
Epon828/IPDA	46.4	112.3	218.7	595
Epon828/DMD	58.3	123.4	223.3	495

Table 3.1. Curing characteristics of the Epon 828/IPDA and Epon 828/DMD systems.

The curing range is higher in the case of the Epon 828/IPDA system compared to the Epon 828/DMD system. The onset temperature for the Epon 828/IPDA system was lower compared to the Epon 828/DMD system. This suggests that the chemical reactivity

of IPDA is higher than DMD, and this makes sense because the steric hindrance of the DMD is higher compared to the IPDA curing agent.

In general, the DSC is operated at moderate curing temperatures, which determines the heat of the curing. To understand further and to optimize the curing temperatures, the first step was to perform dynamic DSC scans at various heating rates. Figures 3.2 (a) and (b) show the DSC thermograms of Epon 828/IPDA and Epon 828/DMD cured at different ramp rates.

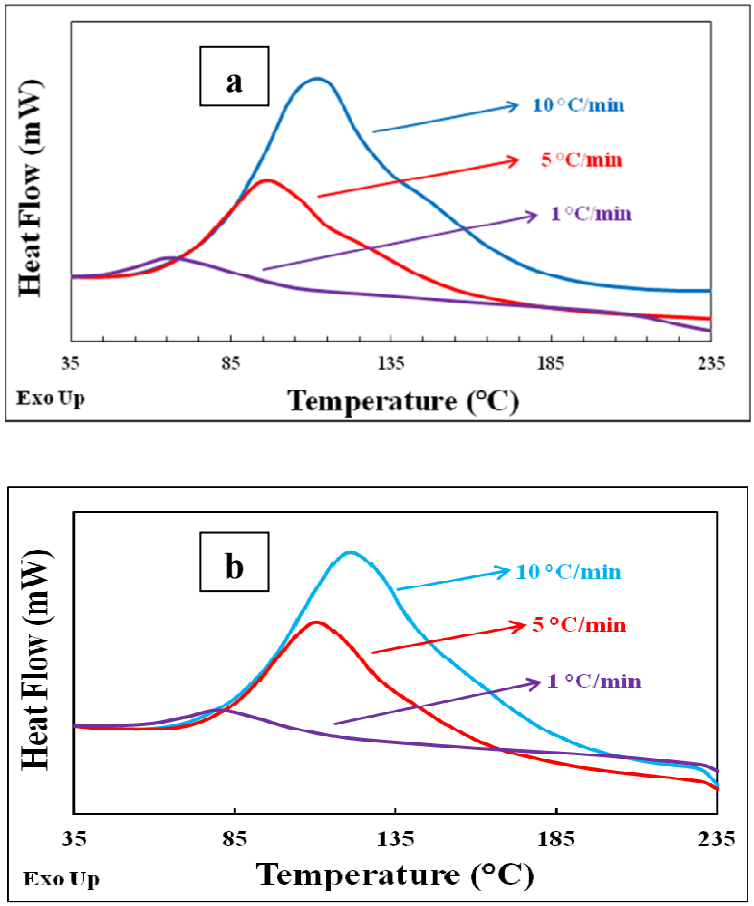

Figure 3.8. DSC curves of (a) Epon 828/IPDA and (b) Epon 828/DMD systems at different heating rates.

The results from the above figure suggested that the exothermic heat evolved at different heating rates was similar in all the cases. Reheating after cooling back to room temperature at 10 °C/min shows the absence of a residual exotherm and suggests completion of curing reaction. Figure 3.3 shows the completion of the curing reaction indicating the glass transition at higher temperature region. The glass transition temperature of this systems was found to be ~145 °C.

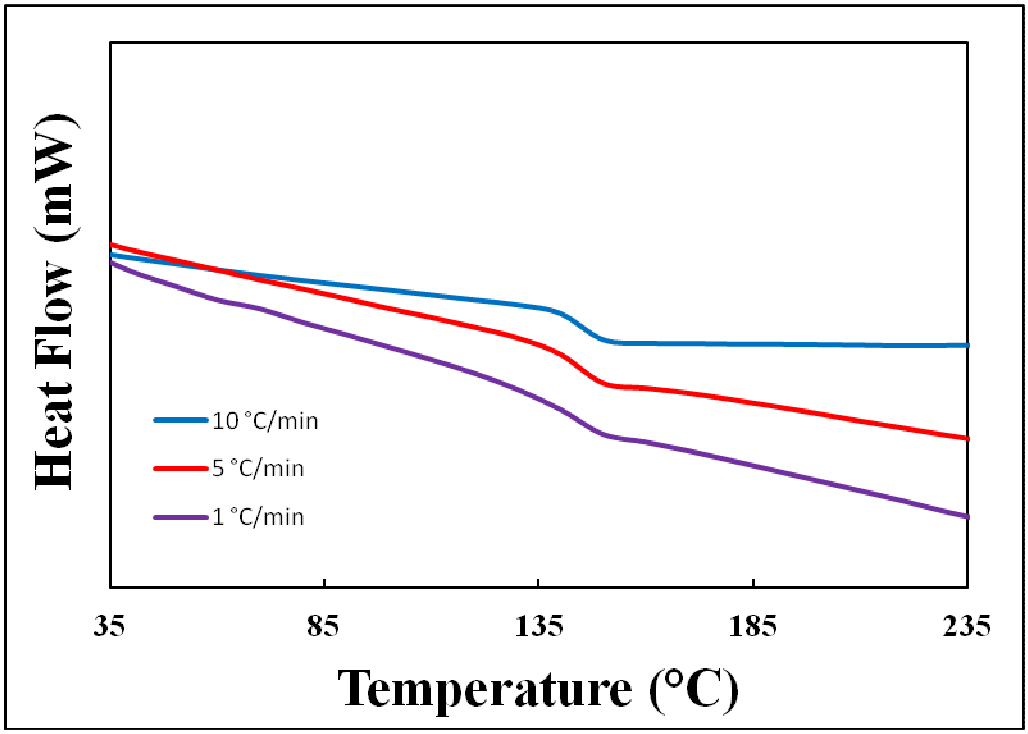

Figure 3.9. T_g curves of Epon 828/IPDA at different heating rates (10,5, 1 °C/min).

In general, a parts per hundred parts resin (PHR) calculation gives the stoichiometric amounts of curing agent needed to cure an epoxy system.

To optimize the amounts of curing agents used in these systems, different stoichiometric amounts listed in Table 1 of the experimental part were studied. Figure

3.4. (a) and (b) showed DSC thermograms which represented the curing of Epon 828 with different amounts of IPDA and DMD curing agents.

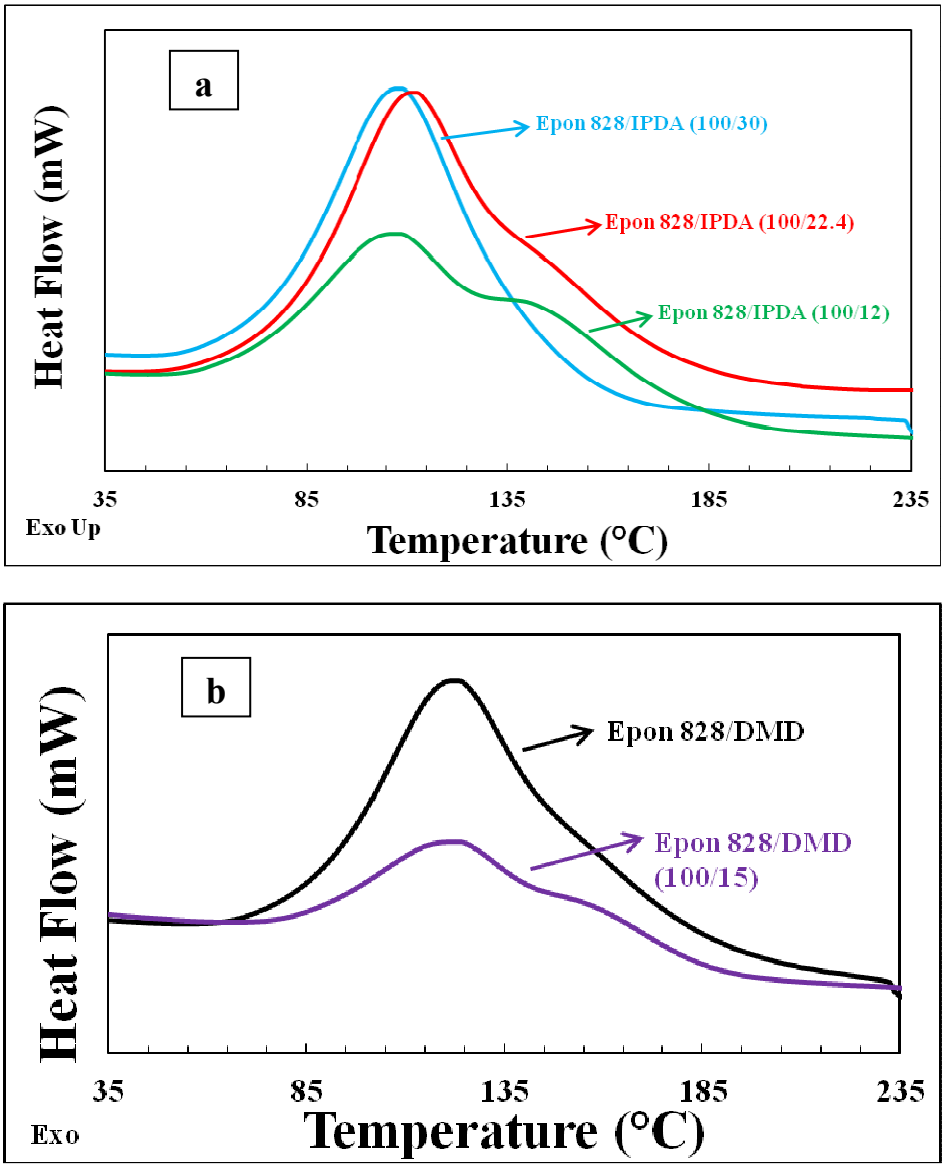

Figure 3.10. DSC curves of (a) Epon 828/IPDA and (b) Epon 828/DMD systems for various amounts of curing agents at 10 °C/min.

Just looking at (a), the blue curve looks like a single transition, whereas all the other curves looks like they have multiple transitions. The reason for this behavior can be explained based on the multiple ratios of reactants used in this system. As stated

earlier PHR determines the stoichiometric ratios of curing agents required to react with epoxy resin. To optimize the amount of curing agent, in this study the curing was performed with excess, PHR, and deficient amount of curing agent. Firstly, in the case of blue curve in Figure (a), there was an excess amount of curing agent IPDA. This suggests that epoxides readily react with primary amines and run out before they are actually able to react with the secondary amines indicating a single transition. Secondly, in the case of the red curve in Figure (a) and the black curve in Figure (b), a stoichiometric amount of curing agent was used. Here, after reaction between primary amine and epoxides, the left over epoxides react with the secondary amine, thus forming a small transition or shoulder at higher temperature region. Thirdly, in the case of the green curve in Figure (a) and purple curve in Figure (b), a deficient amount of curing agent was used. Therefore, all primary amines will get reacted and get exhausted, thus absolutely all secondary amines will react, resulting in a stronger peak around higher temperature region.

The heat evolved by the system will be directly proportional to the number of reactive groups consumed in the reaction. The results suggest that exothermic heat for Epon 828/IPDA cured when a stoichiometric ratio of 100/22.4 used was higher compared to all other concentrations. In a similar way, the exothermic heat in the Epon 828/DMD cured at 100/30 ratio was higher compared to other concentrations.

The glass transition temperature of the samples was obtained by reheating (second heating) the samples at 10 °C/min after the first cycle of exotherm. Figure 3.5 shows the glass transition temperature obtained for Epon 828/IPDA systems at different stoichiometric ratios.

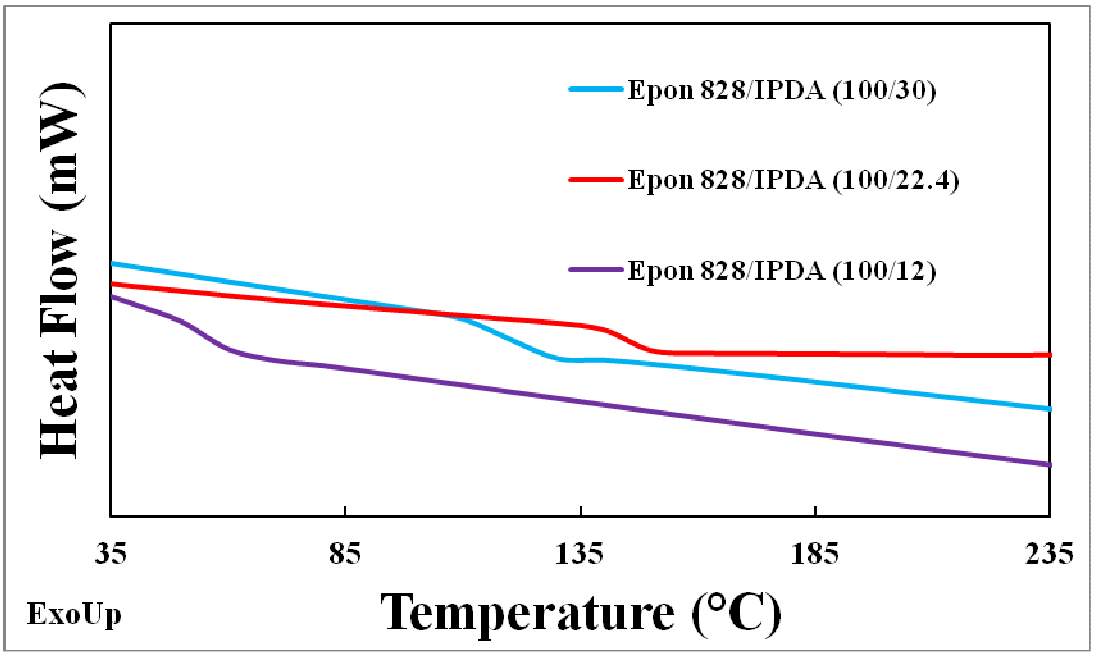

Figure 3.11. T_g curves Epon 828/IPDA cured at various amounts of curing agents at 10 °C/min.

From the above figure the glass transition temperature (T_g) obtained in the Epon 828/IPDA cured at 100/22.4 was higher compared to all stoichiometric ratios. The reason for this behavior may be, in the first case, the excess amine might act as plasticizer. Where plasticizers are defined as molecules that are added to soften a polymer by reducing its crystallinity or glass transition temperature. Whereas in a second case, there is not sufficient amine to completely cure epoxy system. To further investigate the curing behavior, the next step was to determine the reason for the appearance of the second peak in the exotherm, observed when epoxy cured with a deficient amount of curing agent.

Curing of epoxy systems proceeds in two steps: (1) addition of primary amine with epoxy and (2) addition of secondary amine with epoxy. From the origins of figure 3.4, it was clear that the diamines of the primary amine react at lower temperature region and secondary amines react at higher temperature region. At this point, it will be useful to

see if we can further probe to find the transition of primary amine at lower temperature compared to secondary amine at higher transition temperature separately. Therefore, to further investigate this behavior, a primary amine (cyclohexylamine) and secondary amine (dicyclohexylamine) were chosen. Figure 3.6 shows the cure behavior of this systems at PHR stoichiometric amounts of curing agent at 1 °C/min heating rate.

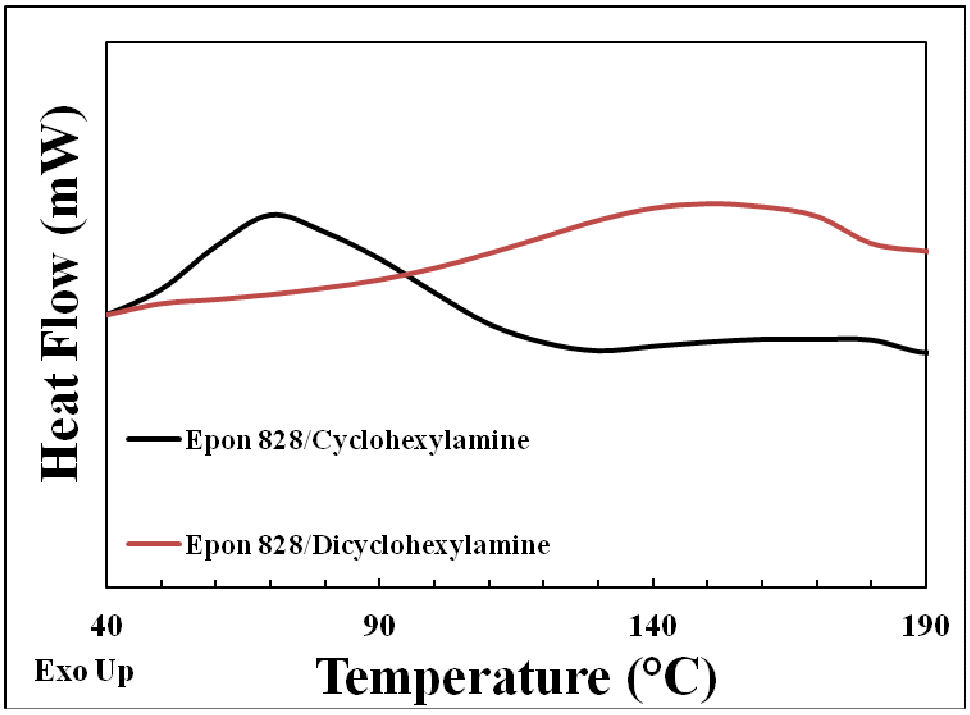

Figure 3.12. DSC thermograms of Epon 828 cured with cyclohexylamine and dicyclohexylamine at 1 °C/min heating rate.

The results suggest that the peak temperature of the primary amine cured epoxy exhibited an exotherm at a lower temperature regime, whereas the peak temperature of the secondary amine cured epoxy exhibited an exotherm at a higher temperature region. The second peak in Figure 3.4 (a) and (b) was intermediate between these two exotherms.

CHAPTER IV

EPOXY/SWNT NANOCOMPOSITES

This part of my research was mainly focused on preparing epoxy/SWNT nanocomposite with the objective to achieve better thermal and mechanical properties. To achieve this goal, we need to maximize dispersion of SWNTs within the epoxy matrix, while monitoring it closely by spectroscopic means and observing the effect of dispersion on the ultimate properties of the prepared nanocomposites.

4.1. Background

SWNT nanocomposites show dramatic mechanical properties improvements at few wt. % loadings. Earlier work paid poor attention to the choice of solvent for dispersion of SWNTs and techniques to monitor the quality of dispersion of the SWNTs in the epoxy matrix.[46,68-70] Earlier work in this study indicates that by, picking a high quality epoxy/ curing agent (Epon 828/IPDA) combination and selecting a better, but less traditional solvent *N*-methylpyrrolidone (NMP) to disperse SWNTs, we saw dramatic improvements in nanocomposites with almost orders-of magnitude at lower loadings.

Later in this study, we developed a novel technique to monitor the quality of dispersion though out the curing process. Applying what we learned from the proof-of-concept into the DGEBF type epoxy, Epon 862/Amicure PACM curing agent system studied in the literature and also by monitoring the dispersion of SWNTs as individuals throughout the curing process studies, we saw impressive improvements in the nanocomposites. To start with, determining the quality of dispersions in solvent we used UV/visible-NIR absorbance spectroscopy.

4.2. UV/visible-NIR absorbance spectroscopy

The dispersion of SWNTs in NMP solvent was monitored by UV/visible-near infrared absorbance spectroscopy. Figure 4.1 shows absorbance spectra of dispersed SWNTs in solvent before and after centrifugation. As shown in absorbance spectra (Figure 4.1) all the optical transitions (E11, E22, M11) are present in the samples. This observation clearly suggests that this technique can be used to monitor the dispersions and SWNTs exists in debundled state in the samples.

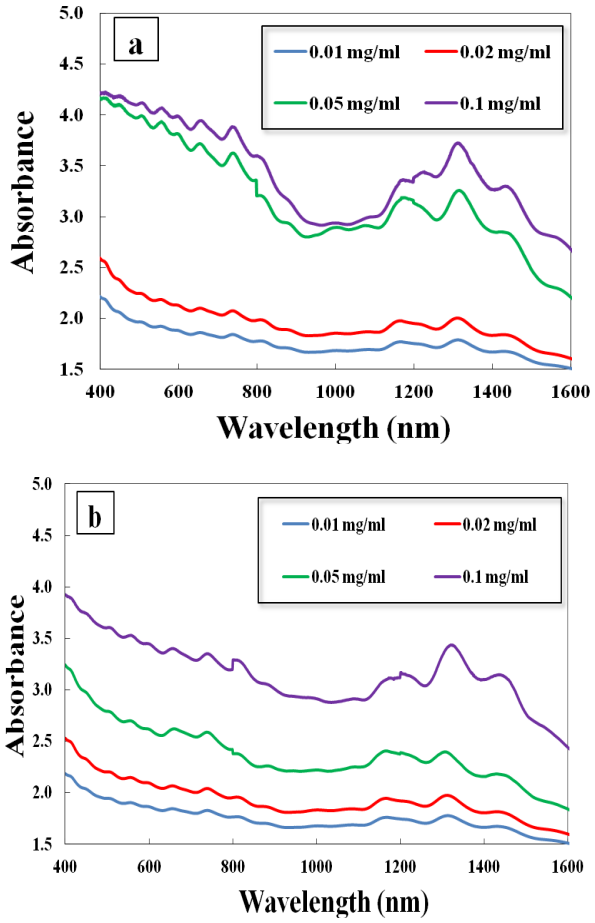

Figure 4.1. Comparison of the SWNTs dispersed in NMP (a) before centrifugation (b) after centrifugation.

After determination of the quality of dispersions, the next step was to quantify the effect of dispersion on the thermal and mechanical properties of the nanocomposites. To further investigate the thermal properties of these composites, differential scanning calorimetry (DSC) and thermogravimetric analysis were performed.

4.3. Differential scanning calorimetry (DSC) analysis

The glass transition (T_g) temperature of the prepared epoxy/SWNT nanocomposites were determined by DSC analysis. Figure 4.2 shows the variation of T_g with different amounts of nanotube loading (0.001-0.004 wt.%). It was found that plain

epoxy composite exhibits a glass transition at 140 °C. As SWNT loading is increased, the T_g showed an increase to a maximum of 147 °C with a loading of 0.004 wt.%. The increase in the glass transition temperature can be attributed to the good quality dispersion of SWNTs in the epoxy matrix.

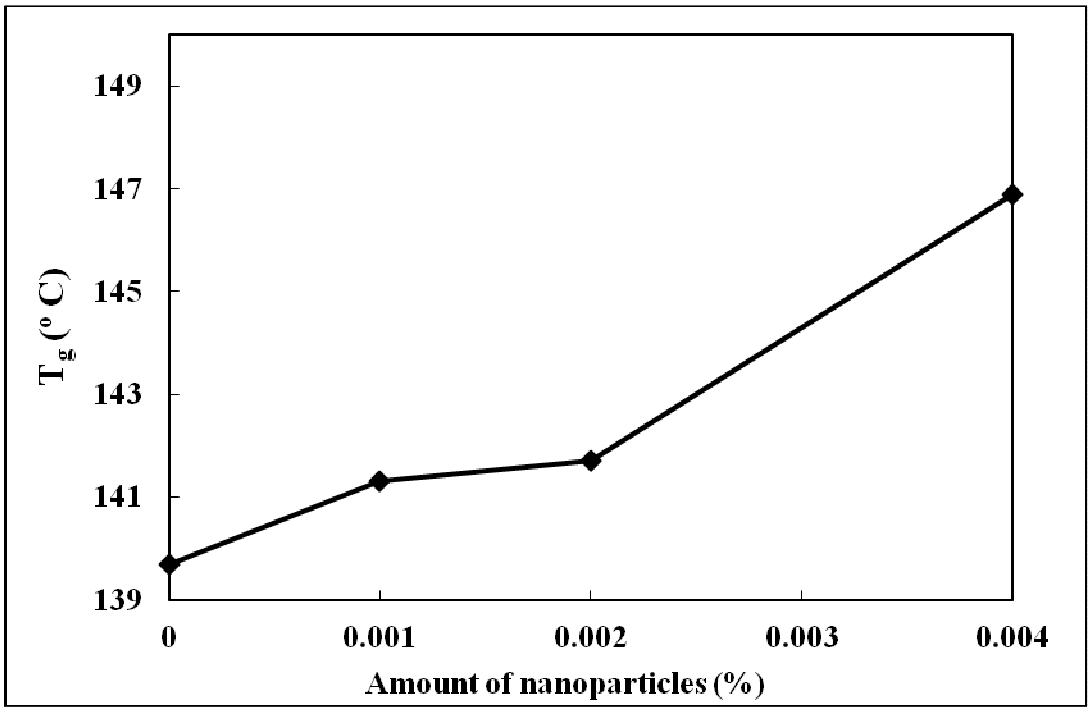

Figure 4.2. Variation of glass transition (T_g) temperature with amount of filler loading.

4.4. Thermogravimetric analysis

Thermal properties of the epoxy/SWNT nanocomposites were determined by TGA. The epoxy nanocomposites showed similar degradation at various concentrations of filler, suggesting that presence of SWNTs does not significantly affect the thermal degradation of the epoxy matrix. Figure 4.3 shows the thermal oxidative behavior of the prepared epoxy nanocomposites. These results suggest that very low loadings of SWNTs are not enough to affect the thermal oxidative degradation of the epoxy matrix.

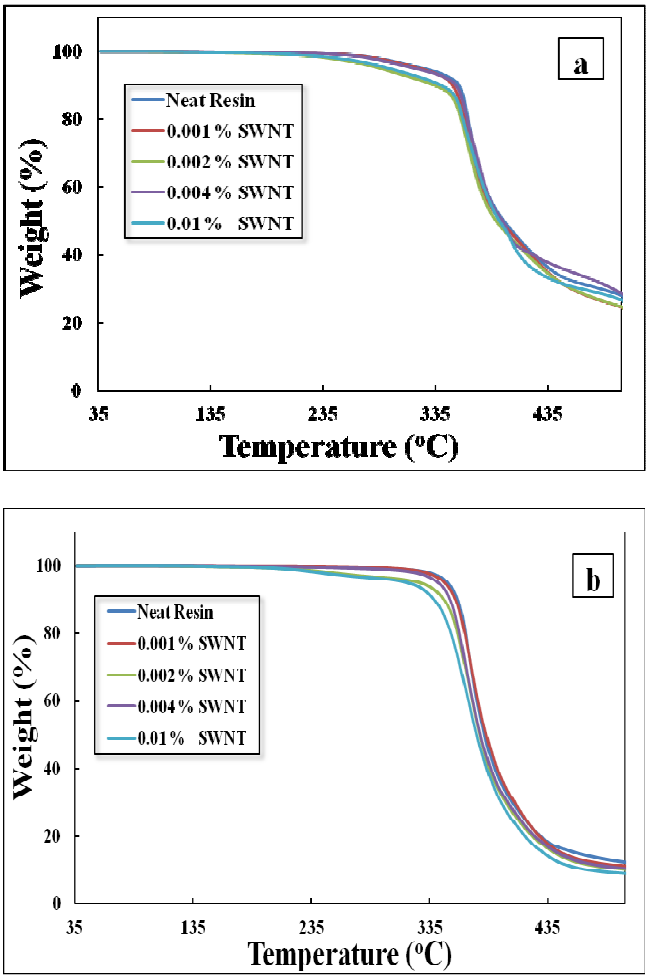

Figure4.3. TGA of neat resin and epoxy/SWNT nanocomposites (a) in air (b) in nitrogen.

4.5. Dynamic mechanical analysis (DMA)

The storage modulus of the prepared epoxy/SWNT nanocomposites were measured by DMA. Figure 4.4 shows the variation of storage modulus with different amounts of nanotube loading (0.001-0.01 wt.%). These data clearly show that the storage modulus of epoxy/SWNT nanocomposite are higher than that of plain epoxy composite. The storage modulus of the plain composite was found to be 2200 MPa. The storage modulus epoxy/SWNT nanocomposite with 0.004 wt.% was found to be 3100 MPa. An increase in 37% of the storage modulus suggests a significant load transfer between the

epoxy matrix and the SWNT filler. Other studies have shown significant improvements in storage modulus only at much higher SWNT loading than were we used in the present study. This suggests that good quality dispersion of the SWNTs, dramatically improves the load transfer behavior.

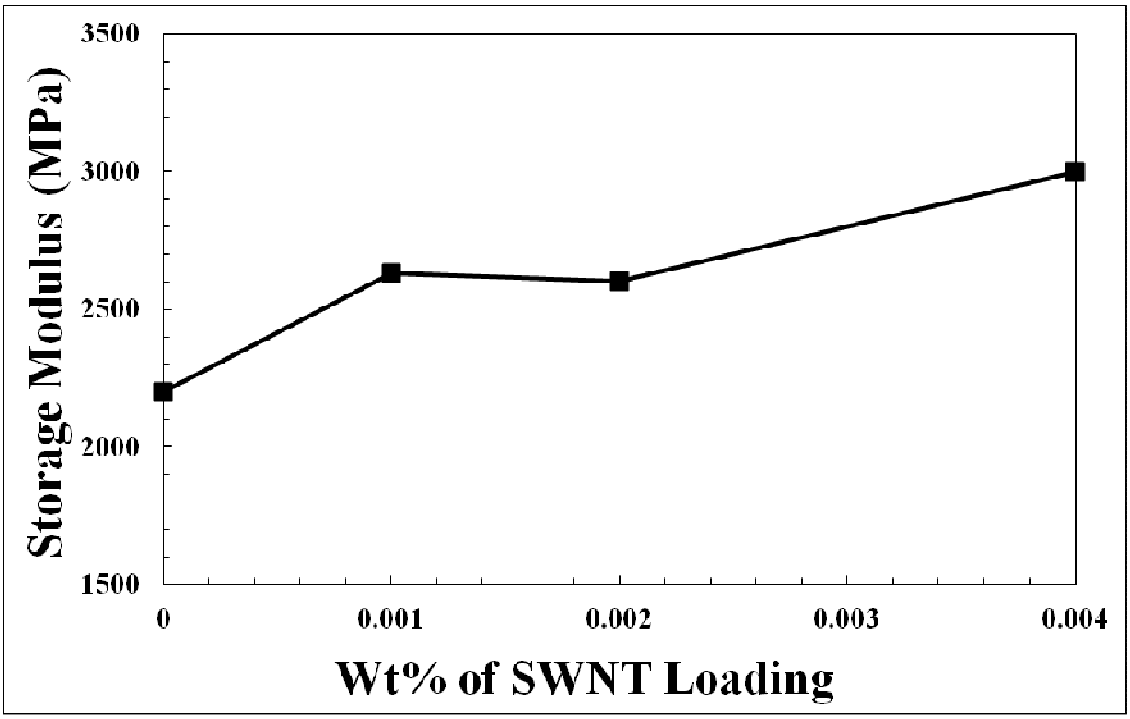

Figure 4.4. Variation of storage modulus with amount of filler loading (0.001-0.01 wt.%).

At this point, we wanted to apply our methodology to an epoxy resin/curing agent system previously studied as a matrix for SWNT composites in the literature to evaluate whether our methodological improvements would result in improved materials properties. Therefore, we decided to change the epoxy system and the curing agent for the following

studies. In this part of study, we used near-infrared fluorescence as a novel technique to estimate the quality of dispersions of SWNTs.

4.6. Near infrared (NIR)-fluorescence spectroscopy

The quality of dispersion of SWNTs in solvents *N*-methylpyrrolidone (NMP), dimethylformamide (DMF) and also upon addition of epoxy matrix were evaluated using NIR-fluorescence spectroscopy. Whereas, the quality of dispersion in cured epoxy nanocomposites were determined using optical microscopic images. NIR-fluorescence is a sensitive, zero background technique to evaluate the quality of SWNT dispersions. Ultrasonication was performed to disperse SWNTs into the solvent. The main goal here was to optimize the ultrasonication conditions to achieve maximum dispersion of individual nanotubes without having any damage to the nanotubes. Figure 4.5 shows the fluorescence of SWNT dispersion in NMP and DMF at 658 nm excitation after ultrasonication.

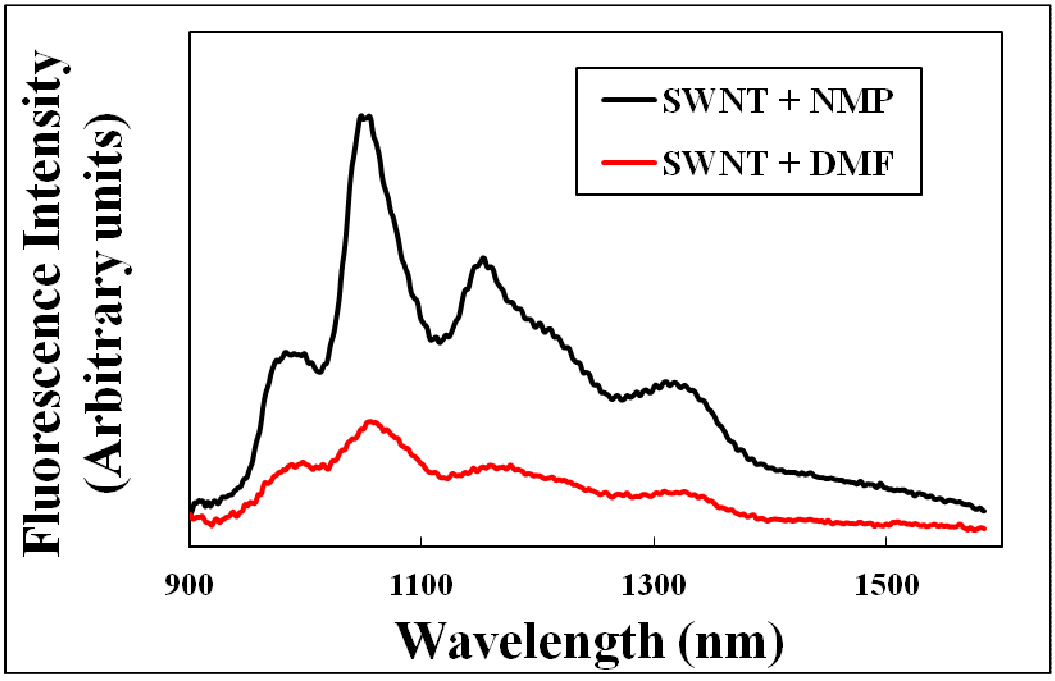

Figure 4.5. SWNT fluorescence taken at 658 nm excitation while dispersed in NMP (black) and DMF (red).

The above figure indicates similar concentration of SWNTs dispersed in NMP and DMF and the fluorescence intensity was higher in the case of SWNTs dispersed in NMP compared to DMF. This result suggests the individual nanotubes are more in NMP compared to DMF. After optimizing conditions to achieve the maximum dispersion in the solvent systems, the next step was to optimize the ultrasonication conditions to achieve good dispersion even upon addition of the epoxy matrix to the solvent system, and this was also monitored by NIR-fluorescence. Figure 4.6 shows the fluorescence spectra of SWNT dispersion after addition of epoxy matrix to the solvent system.

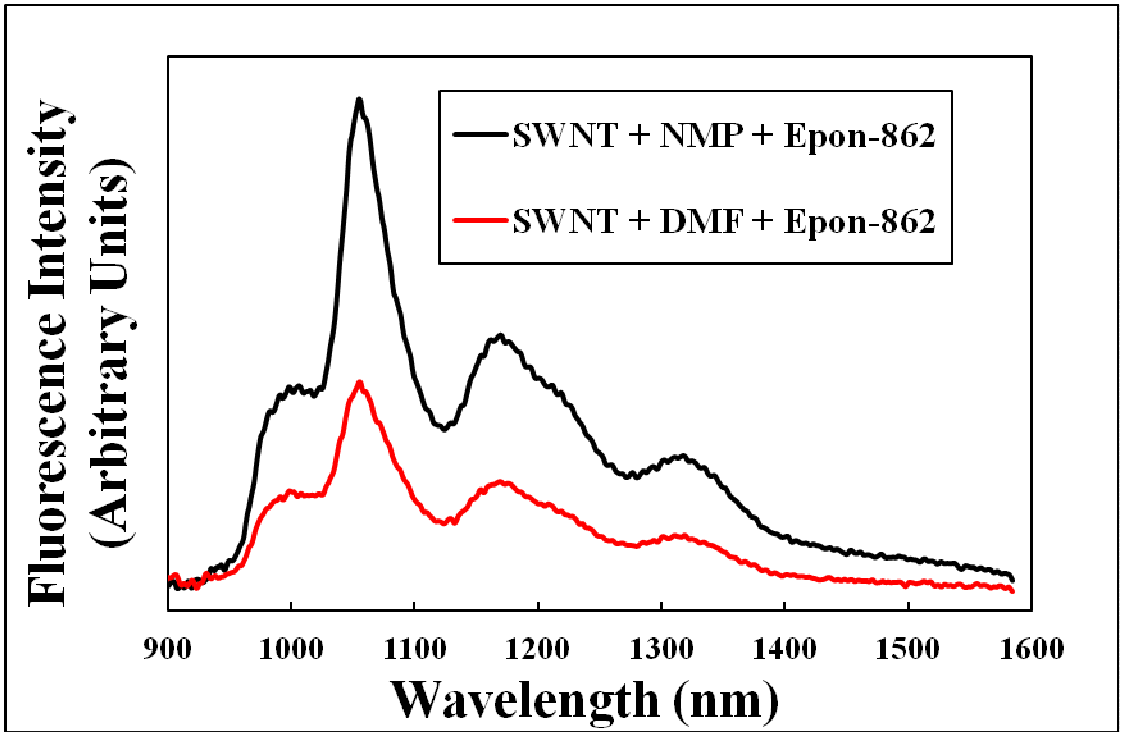

Figure 4.6. SWNT fluorescence taken at 658 nm excitation with addition of Epon-862 to NMP (black) and DMF (red) dispersions.

The increase in the fluorescence intensity indicates the growth in individual nanotubes in the case of epoxy nanocomposites, where the initial dispersion was in NMP compared to DMF solvent.

SWNTs exists primarily in two forms: metallic and semiconductors. An individual semiconductor nanotube gives fluorescence. Peak positions are sensitive to the nanotube environment in the fluorescence. Figure 4.7 shows the fluorescence spectra of SWNTs dispersed in NMP solvent with and without added epoxy matrix.

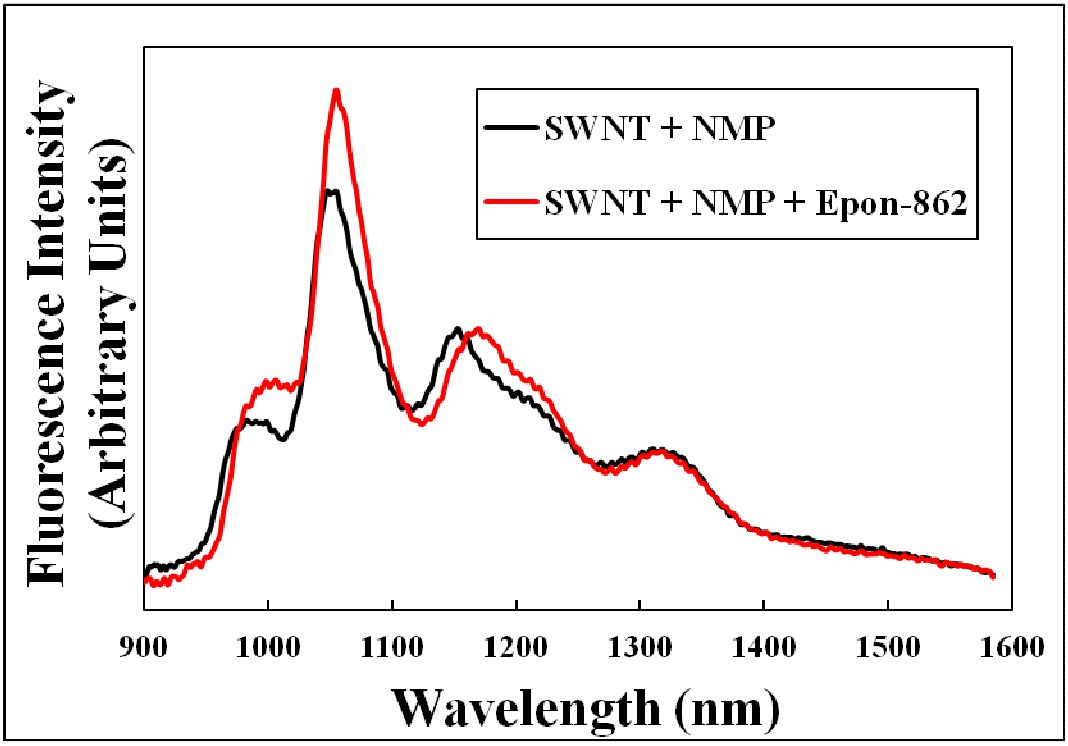

Figure 4.7. SWNT fluorescence taken at 658 nm excitation without addition (black) and with addition of Epon-862 to NMP dispersions.

The above figure clearly indicates a shift in the peak position upon addition of epon-862 into solvent system, suggesting a change in the nanotube environment after

addition of the epoxy system. Previous work done by Lau, et al[46] demonstrated that the amount of residual solvent present in the nanocomposites affected the mechanical properties of the prepared epoxy nanocomposites. Therefore, determining the presence of residual solvent in the composites plays a significant role in determining the thermo-mechanical properties of epoxy nanocomposites.

4.7. Thermogravimetric analysis (TGA)

The presence of residual solvent in the epoxy matrices before curing was determined using thermogravimetric analysis (TGA). Figure 4.8 shows the amount of residual solvent present in the epoxy matrix before curing.

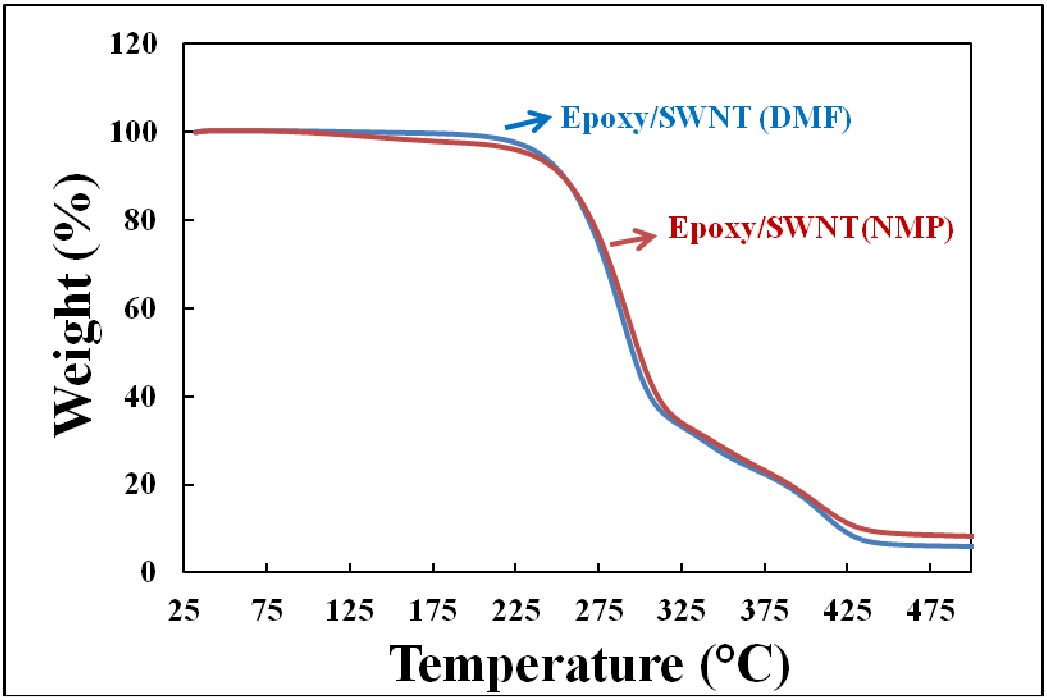

Figure 4.8. TGA analysis of SWNT/epoxy composite at different loadings ranging from 0.001 wt%-0.01 wt%.

The weight loss from 150-235 °C is attributed to the evaporation of the DMF (b.p. 150 °C) and NMP (b.p. 201 °C) solvent. The weight loss between 235-500 °C is ascribed to the decomposition of nanotube/epoxy composites. The above figure clearly suggests no decomposition for sample prepared using DMF solvent. The sample prepared using NMP showed a small decomposition (less than 5%), clearly demonstrating removal of solvent in the prepared matrices. The relative higher fraction of weight loss in the case of NMP solvent prepared sample showed poor storage modulus of the composites compared to DMF prepared nanocomposites. To further estimate the quality of dispersions in the cured epoxy nanocomposites, optical microscopic images of the samples were observed.

4.8. Optical Microscope Images

The selection of proper solvent for preparation of epoxy nanocomposites plays a significant role in two aspects: A) dispersion of SWNT bundle into individuals B) maintenance of the stable dispersion throughout the curing process, because SWNT tend to agglomerate again due to van der Waals forces.

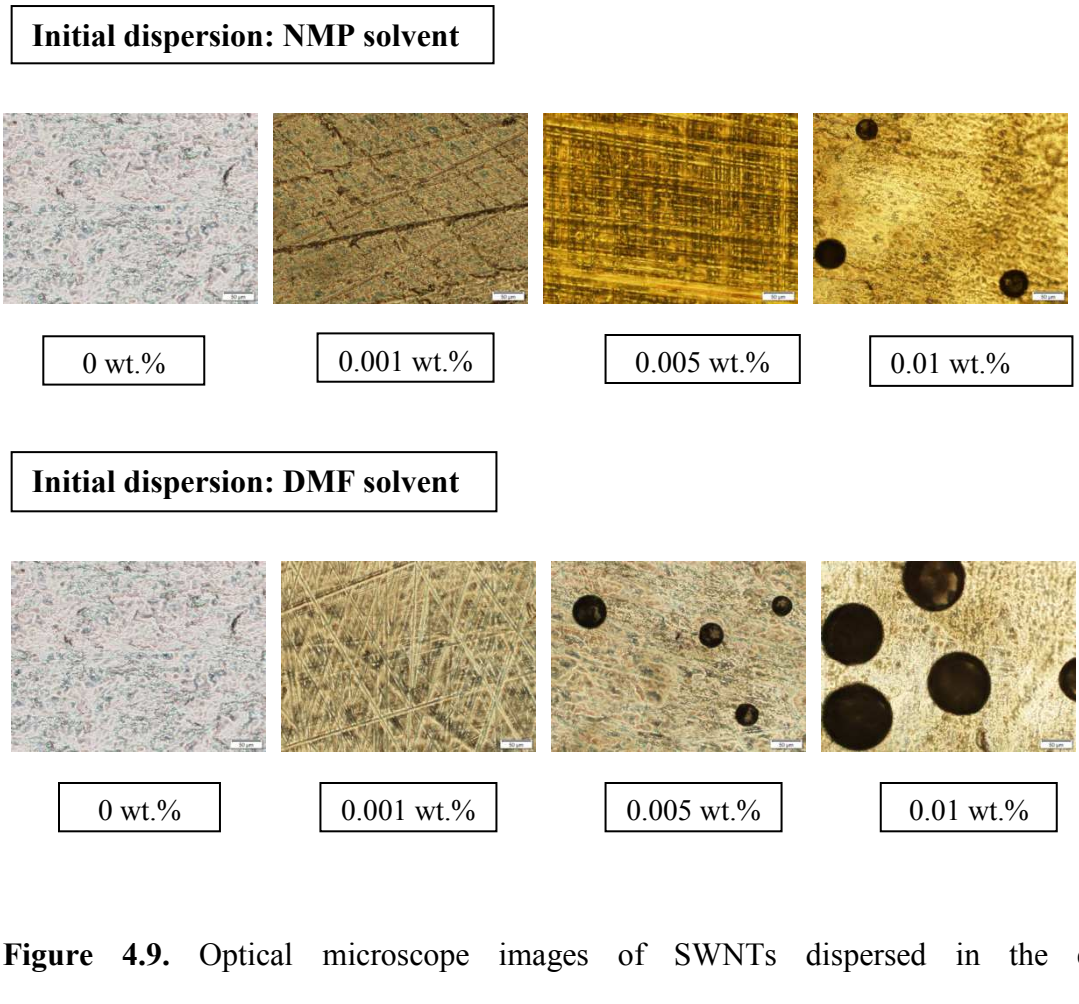

Figure 4.9. Optical microscope images of SWNTs dispersed in the epoxy nanocomposites.

The absence of agglomeration indicates the uniform dispersion of SWNTs in the prepared nanocomposites. The SWNTs tend to agglomerate at 0.01 wt. % in the case of nanocomposites prepared using NMP for initial dispersion, whereas they tend to aggregate at even lower concentration i.e. at 0.005 wt.% in the case of nanocomposites prepared using DMF for initial dispersion. This clearly demonstrates that there is a higher saturation point for dispersion of SWNTs that exists in the case of NMP compared to DMF solvent. These results were consistent with the earlier work done by Ausman, et

al[71] demonstrating that SWNTs are more individuals in the case of NMP compared to DMF solvent. The level of dispersion of SWNTs and the presence of residual solvent in the prepared nanocomposites are the two factors that show impact on improvement of thermal and mechanical properties of nanocomposites.

After monitoring the quality of dispersion and the amount of residual solvent our next goal was to determine the effect of this dispersion on the mechanical properties of the epoxy nanocomposites. Dynamic mechanical analysis is a powerful technique to measure the viscoelastic properties of the nanocomposites under cyclic stress.

4.9. Dynamic mechanical analysis (DMA)

Storage modulus of the epoxy nanocomposites were evaluated using DMA. The variation of storage modulus at different nanotube loading ranging from 0.001-0.01 wt.% dispersed in two different solvents (NMP and DMF) are shown in Figure 4.10. At room temperature, the epoxy nanocomposites showed a higher storage modulus compared to the plain epoxy composite. The average storage modulus value of the plain epoxy composite as measured was 2420 MPa. Epoxy nanocomposite prepared at 0.005 wt.% nanotube loading (initial dispersion: DMF) showed an average storage modulus of 2873 MPa. An increase of about 19% in the storage modulus was observed for nanocomposites prepared using initial DMF dispersion compared to plain epoxy composite. Epoxy nanocomposite prepared at 0.01 wt.% nanotube loading (initial dispersion: NMP) showed an average storage modulus of 2766 MPa. An increase of about 14% of storage modulus was observed for nanocomposite prepared using initial NMP dispersion compared to plain epoxy composite. The lower increase in the storage modulus in the case of NMP

dispersed samples may be due to the small amounts of residual solvent trapped in the prepared epoxy nanocomposites determined by TGA.

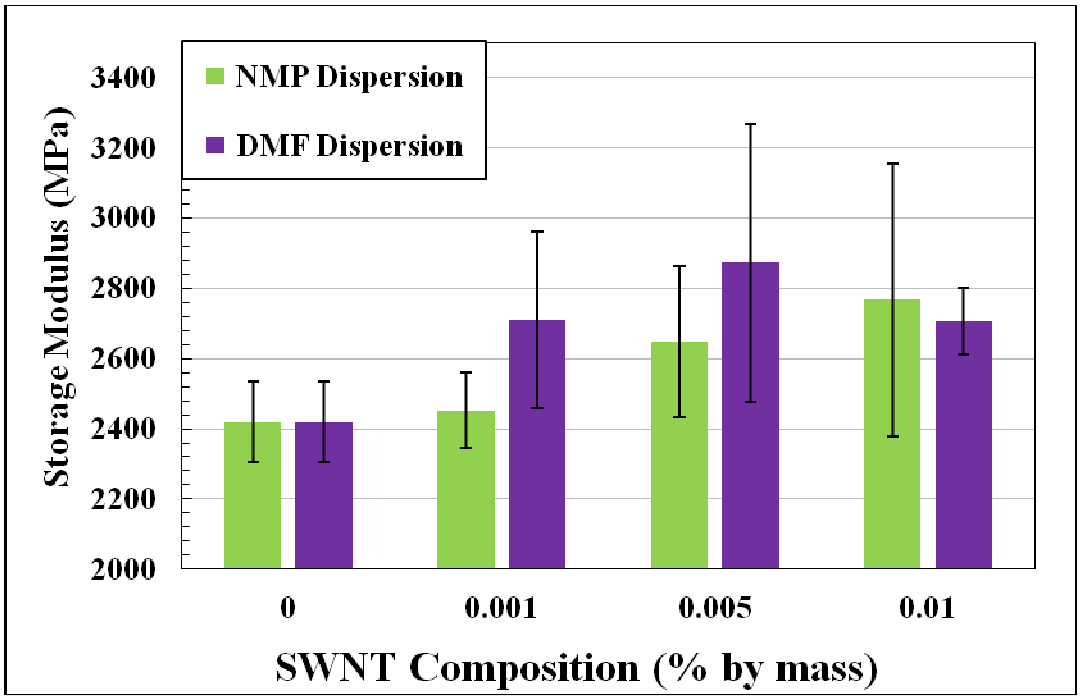

Figure 4.10. Storage modulus of epoxy nanocomposites at various loadings (0.001-0.01wt. %) of SWNTs.

To determine the effect of dispersed SWNTs on the hydrophobicity of the epoxy composites contact angle measurements were performed.

4.10. Contact angle

The static contact angles for various epoxy/SWNT nanocomposites ranging from 0.001-0.01 wt.% nanotube loading using NMP and DMF as the solvents for the initial dispersion were determined. Figure 4.11 shows the contact angle measured in various prepared epoxy nanocomposites. The nanocomposites prepared by initial dispersion using

DMF had shown significant increase in the hydrophobicity compared to plain epoxy composites. A similar trend was also observed in the samples prepared using NMP as the solvent for initial dispersion.

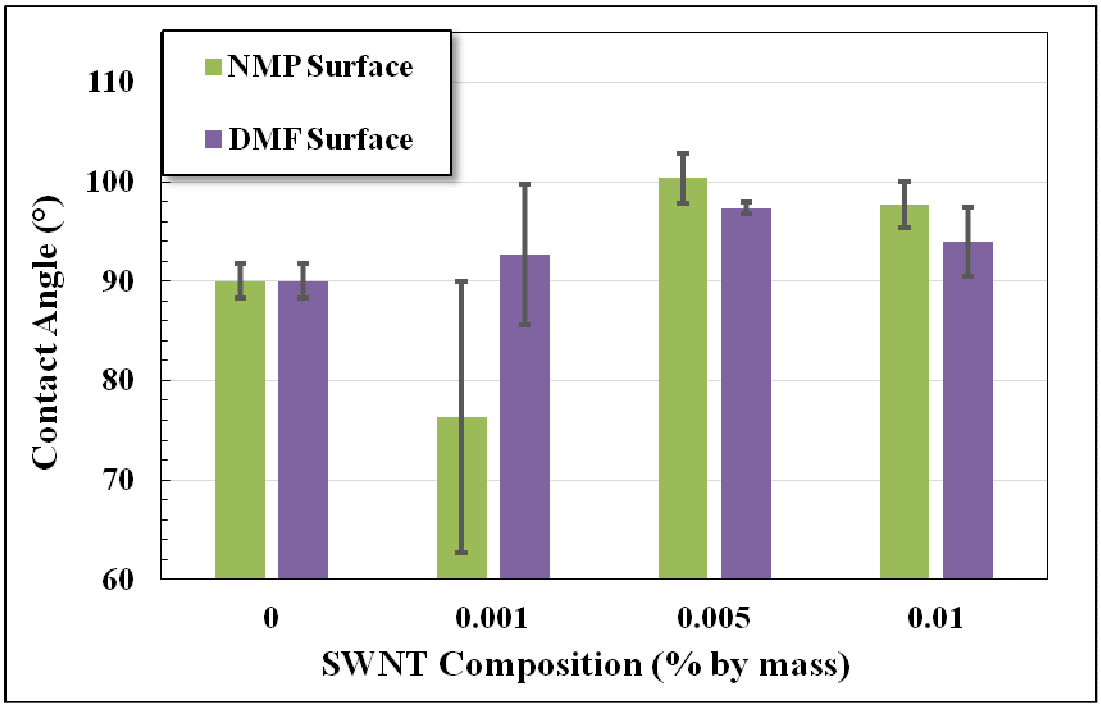

Figure 4.11. Contact Angle of epoxy nanocomposites at various loadings (0.001-0.01wt.%) of SWNTs.

SWNTs in general are more hydrophobic compared to the epoxy composites. The increase in hydrophobicity of the prepared epoxy nanocomposites compared to the plain epoxy composite at various loadings may be attributed to the hydrophobic nature of the dispersed SWNTs.

CHAPTER V

MnO_2 NANOSTRUCTURES FOR CATALYSIS

In a collaborative project with the Bunce group, we were trying to determine the structural differences that resulted in the catalytic activity of three types of MnO_2. The catalytic activities of the compounds were studied based on the oxidation of arylmethylene compounds. The most natural first assumption for catalytic activity is that higher surface area should correlate with higher activity, so that was the parameter we investigated first.

5.1. Brunauer-Emmett-Teller (BET) Analysis

The surface areas of the prepared nano-MnO_2, Attenburrow MnO_2 and commercial MnO_2 were measured using a Quanta Chrome multi point BET method.[72] Table 5.1 lists the surface areas of the samples.

Samples	Surface area (m^2/g)
Commercial-MnO_2	97
Attenburrow- MnO_2	47
Nano- MnO_2	169

Table 5.1. BET surface areas of commercial MnO_2, Attenburrow MnO_2 and nano-MnO_2.

BET surface area results suggested that nano-MnO_2 had higher surface area compared to commercial MnO_2 and Attenburrow MnO_2. Unexpectedly, the BET surface area did not correlate directly with the observed catalytic activity of these samples.

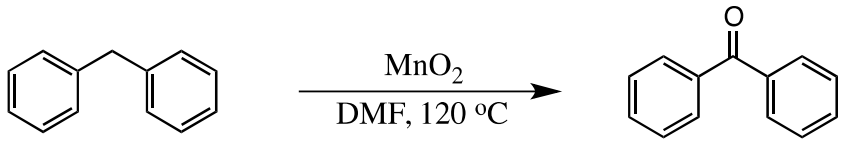

Substrate	Yield (%)
Commercial MnO_2	56
Attenburrow MnO_2	81
Nano MnO_2	95

Table 5.2. Oxidation of diphenylmethane to benzophenone using three different MnO_2 samples.

To further investigate the surface morphology of these catalysts SEM analysis was performed.

5.2. Scanning Electron Microscopy (SEM) Analysis

The surface morphology of the prepared nano-MnO_2, Attenburrow MnO_2, were compared with commercial MnO_2 by SEM analysis. Figure 5.1 represents the SEM images of the nano-MnO_2, Attenburrow MnO_2 and commercial MnO_2.

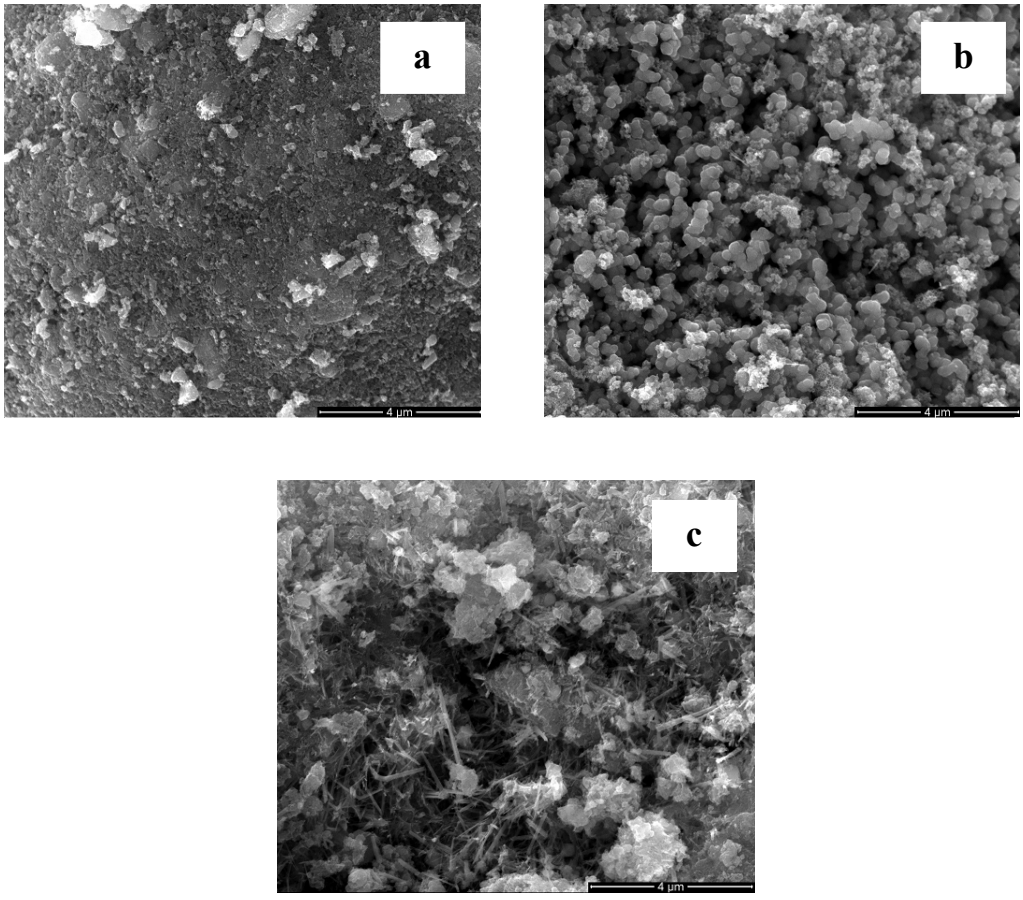

Figure 5.1. SEM images of the (a) commercial MnO_2 (b) Attenburrow MnO_2 and (c) nano-MnO_2.

As shown in Figure 5.1 (a) SEM images revealed that commercial MnO_2 has a plain surface with no observable porosity at the SEM resolution. Figure 5.1 (b) revealed that Attenburrow MnO_2 possesses spherical structures with some porosity in them. Figure 5.1 (c) showed that nano-MnO_2 has high porosity and a nanorod like structures with diameters ranging from 10-50 nm. These results suggest that nano-MnO_2 possesses a higher surface area and porosity compared to Attenburrow MnO_2 and commercial MnO_2. These morphological observations differed from the BET data, where the commercial MnO_2 showed higher surface area than is apparent by SEM. Perhaps the commercial MnO_2 has porosity of a size-scale that is too small to be easily observed by SEM. To study the thermal properties such as water content and decomposition of these catalysts thermogravimetric analysis was performed.

5.3. Thermogravimetric analysis (TGA)

The surface-bound water content of nano-MnO_2, Attenburrow MnO_2, and commercial MnO_2 was measured by TGA. Figure 5.2 shows the TGA curves of nano-MnO_2, Attenburrow MnO_2 and commercial MnO_2. The first weight loss over a temperature range of 100-150 °C is attributed to loss of surface-bound water and the second weight loss over a temperature range of 150-450 °C is attributed to loss of structural water.

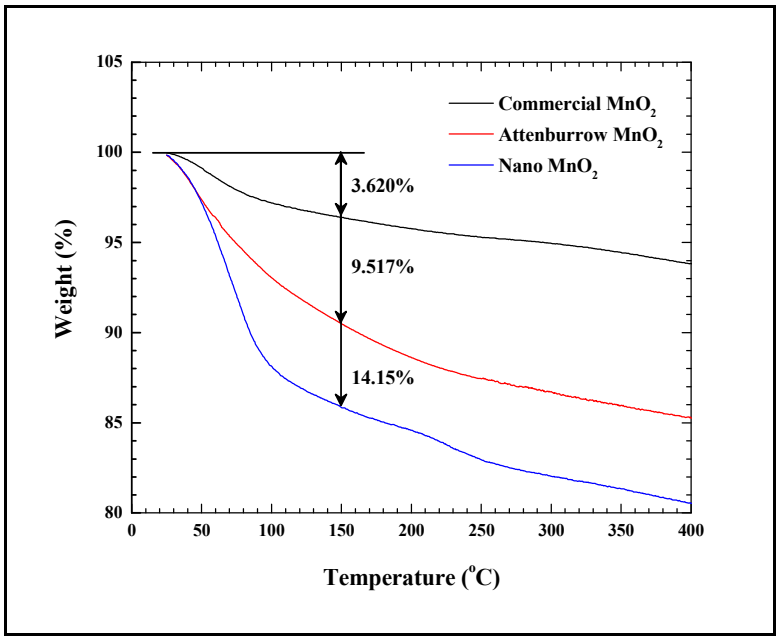

Figure 5.2. TGA curves of MnO_2 samples.

The results suggested that nano-MnO_2 showed a mass loss of 14.2% over a temperature range 100-150 °C, whereas Attenburrow MnO_2 and commercial MnO_2 showed mass losses of 9.2% and 3.6%, respectively. The surface water content, measured by TGA was found to closely correlate with the activity of the reagent. Figure 5.3 shows a correlation that was observed between the surface water content and reactivity of MnO_2 samples.

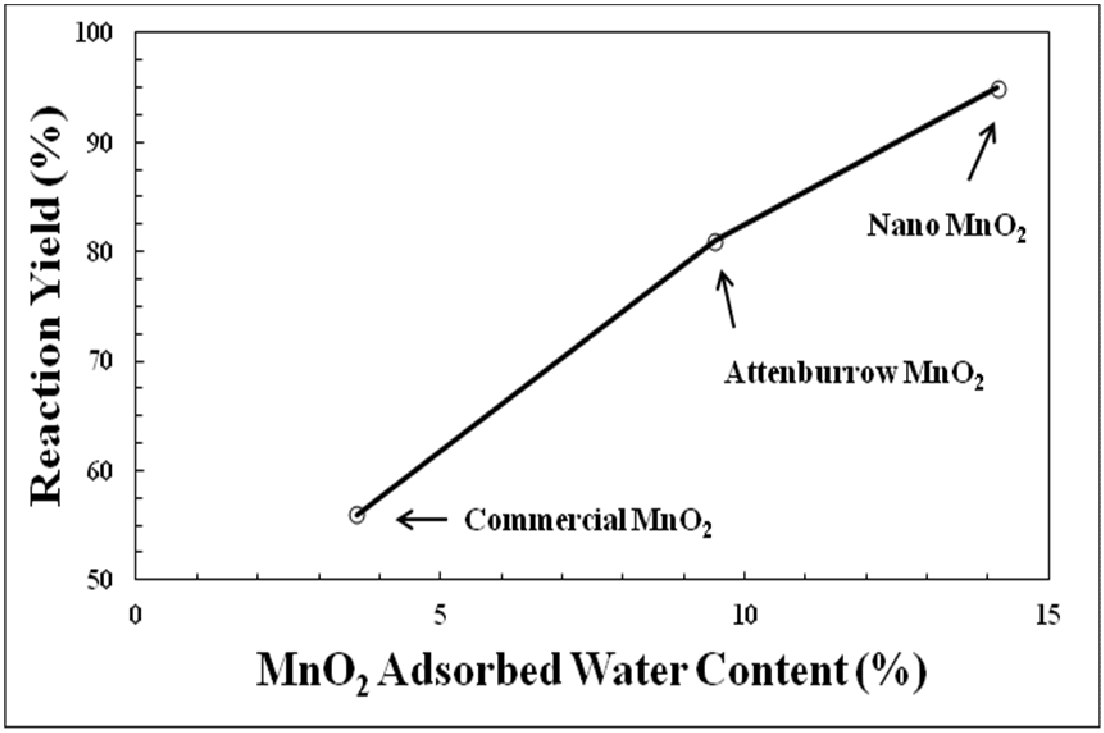

Figure 5.3. Correlation of MnO_2 surface water content with reactivity.

Preliminary results suggested that nano-MnO_2, due to its higher surface area and porosity, retains more adsorbed water and exhibits higher reactivity compared to Attenburrow and commercial MnO_2.[54]

So, while adsorbed water content correlated directly with reactivity, it was unclear whether this was the only relevant characteristic or whether other factors, such as crystal form, could play a complementary role. To further investigate these issues, we synthesized separate samples of the three main crystalline forms of MnO_2, α-, β-, and γ-, by a hydrothermal method. These samples were characterized, and their catalytic activity was compared based on the oxidation of diphenylmethane to benzophenone, a system that showed great resolving-power among the various catalysts in the original study.

5.4. Powder X-ray diffraction (XRD) Analysis

The crystal phase of the three different forms of samples was analyzed by powder X-ray diffraction. Figure 5.4 shows the XRD patterns of α-, β-, and γ-MnO_2 samples. The reflections of the XRD pattern in Figure 5.4, bottom can be indexed to pure tetragonal phase of β-MnO_2 [(space group: P42/mnm (136)] with lattice constants a = 4.398 Å and c = 2.873 Å (PDF # 01-071-0071), which were in good agreement with the reported data for pure phase of β-MnO_2,[57] with lattice constants a = 4.399 Å and c = 2.874 Å (JCPDS 24-0735).

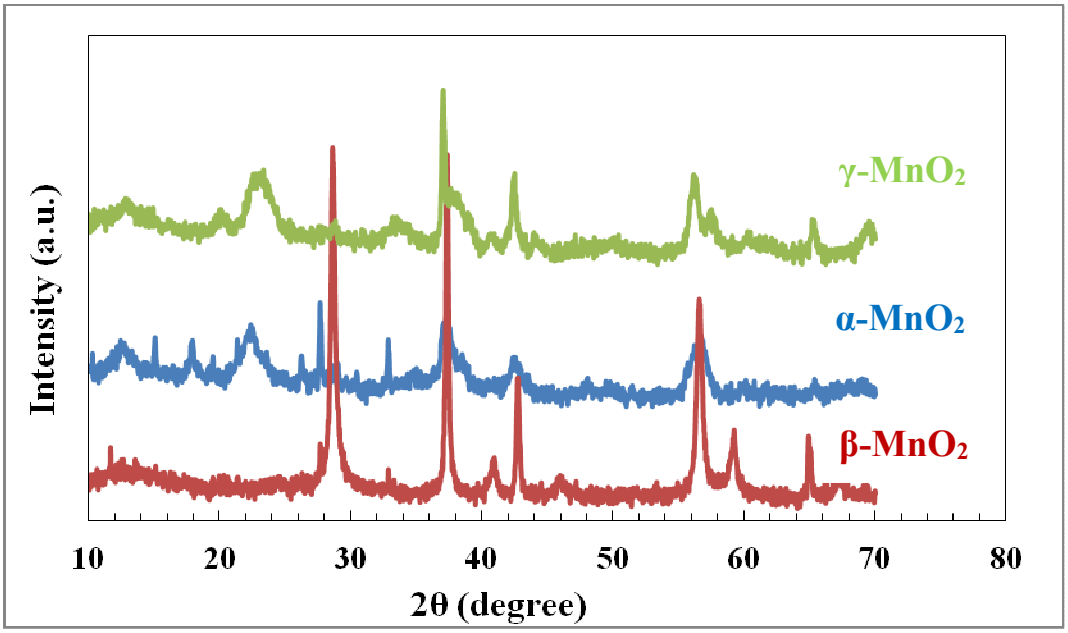

Figure 5.4. Powder x-ray diffraction (XRD) pattern of the as-prepared α-, β-, γ-MnO_2 samples

The XRD pattern in Figure 5.4, middle can be indexed to pure tetragonal phase of α-MnO_2 [(space group: I4/m (87)] with lattice constants a = 9.7847 Å and c = 2.863 Å (JCPDS 44-0141) and the pattern in Figure 5.4, top can be indexed to pure orthorhombic

phase of γ-MnO_2 with lattice constants a = 6.36 Å b = 10.15 Å and c = 4.09 Å (JCPDS 14-0644). Therefore, XRD data clearly demonstrates that we have successfully synthesized samples each of three major structures of MnO_2. It is evident from the diffraction peaks that β-MnO_2 has good crystallinity compared to that of α- and γ MnO_2

5.5 Thermogravimetric analysis (TGA)

The structural water content of the materials (α-, β-, and γ-MnO_2) synthesized in this study was determined by TGA. Figure 5.5 shows the TGA curves for the three crystalline forms of MnO_2. Results suggest that α-MnO_2 contains significantly more adsorbed water compared to other crystalline forms (β- and γ-MnO_2). The reason for α-MnO_2 to hold more adsorbed water can be explained based on its crystal structure.

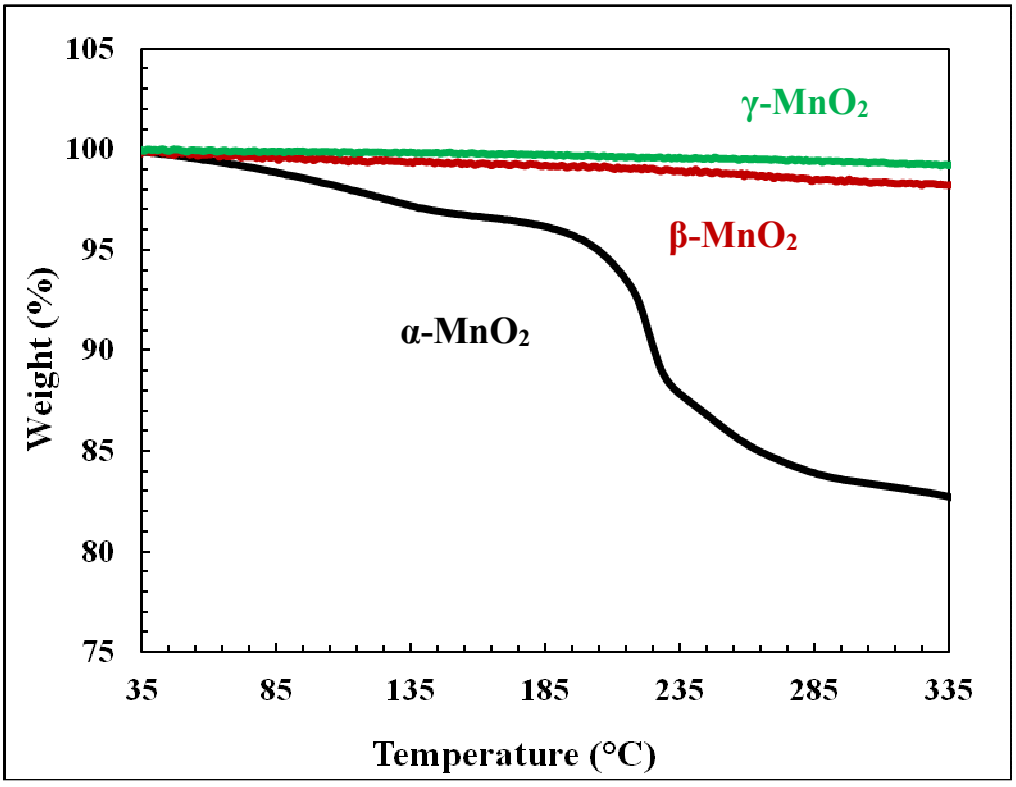

Figure 5.5. TGA results for different crystalline forms of MnO_2 samples

α-MnO_2 due to its (2x2) tunnel structure compared to β- MnO_2 (1x1) and γ-MnO_2 (1x2) can hold H_2O molecules. Earlier studies showed that the higher the adsorbed water content greater the catalytic activity of the material. Therefore α-MnO_2 is expected to show higher catalytic activity for the oxidation of diphenylmethane compared to other crystalline forms.

5.6 Brunauer-Emmett-Teller (BET) Analysis

The surface areas of the as-synthesized different crystalline forms of MnO_2 were measured using a Quanta Chrome multi-point BET method. Table 5.3 lists the surface areas of the synthesized samples.

Samples	**Surface area (m^2/g)**
α-MnO_2	18.00
β- MnO_2	36.20
γ- MnO_2	11.60

Table 5.3. BET surface area of α-, β-, and γ-MnO_2 nanostructures.

The BET surface area results suggests that surface areas are in the order of β-MnO_2 > α-MnO_2 > γ- MnO_2 samples.

5.7. Fourier transform infrared (FTIR) spectroscopy

The purity and chemical composition of the prepared different crystalline forms of MnO_2 were further investigated using FTIR spectroscopy. Figure 5.6 shows the FTIR spectra of the three forms of MnO_2.

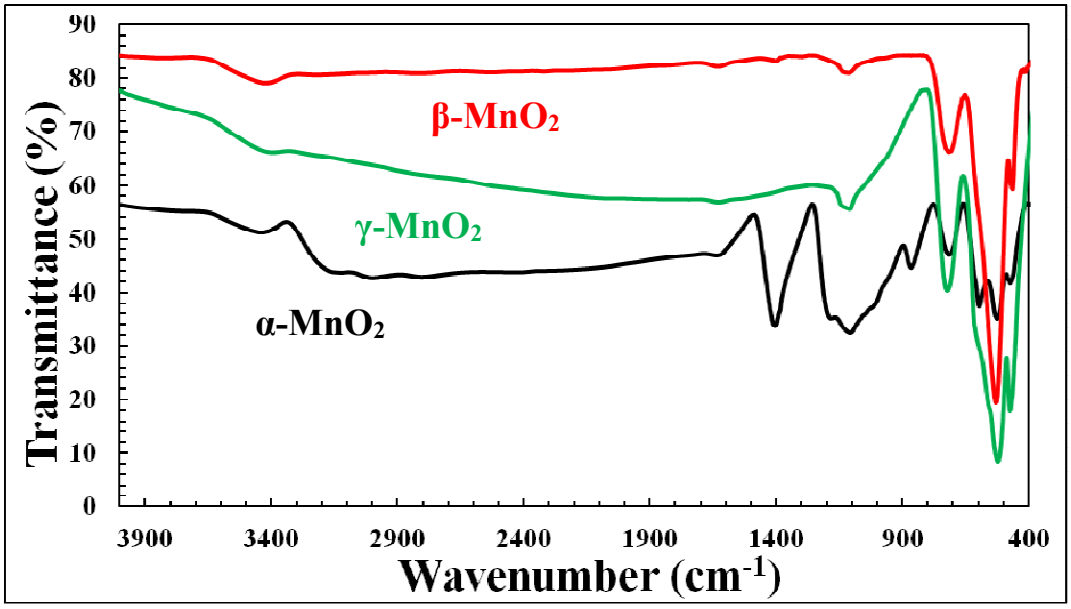

Figure 5.6. FTIR spectra of the as-prepared α-, β-, γ-MnO_2 samples

The absorption bands around 520 and 715 cm^{-1} were assigned to the vibration of Mn-O bond. The absorption bands around 3400 cm^{-1} are due to the absorbed water.

5.8 Scanning electron microscopy (SEM) analysis

The particle size and morphology of the different crystallographic forms of MnO_2 samples were determined using SEM analysis. Figure 5.7 shows the representative SEM images of α-, β-, γ-MnO_2. The difference in the crystallographic phases is seen in the shape, length and diameters of nanowires and nanorods. As shown in Figure. 5.7 (a), α-MnO_2 consists of nanowires with diameters of 10-50 nm with lengths of several

micrometers. The SEM images in Figure 5.7 (b) reveal that β-MnO_2 comprises of nanorods, with square cross-sectional structures with diameters ranging from 40-150 nm and lengths ranging from 2-5 μm. Whereas SEM images in Figure 5.7 (c) reveal mostly nanorods with occasional six-armed star-like structures of γ-MnO_2 with diameters ranging from 30-90 nm and lengths of several micrometers.

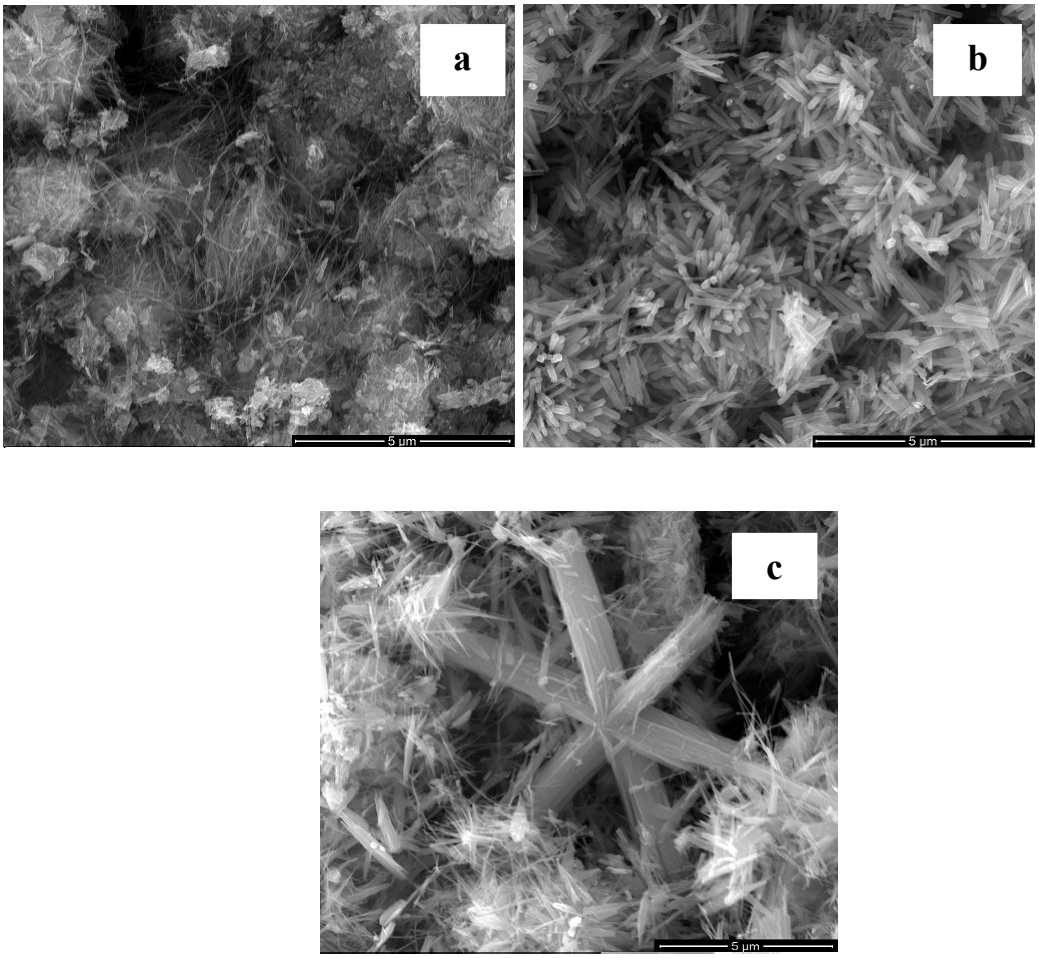

Figure 5.7. SEM images of the as-prepared (a) α- (b) β- and (c) γ-MnO_2 samples

The samples with different physical and thermal properties were used to study the oxidation of diphenylmethane to benzophenone and compare their yields as a result of their morphology, phases, structure and water content.

5.9 Catalytic Activity

The resulting three samples were compared with respect to their catalytic activity for oxidation of diphenylmethane to benzophenone. The two separate samples of each form of MnO_2 were dried at different temperatures (90 and 120 °C), and their differing catalytic activity was compared. These reactions were performed under various conditions including aerobic conditions (under O_2 atmosphere), atmospheric conditions (in air) and anaerobic conditions (under N_2 atmosphere).

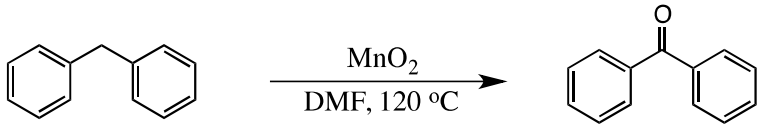

Table 5.4

Substrate	**Drying Temp[a]**	**Reaction Temp**	**Yield**		
			Aerobic (under O_2)	**Air**	**Anaerobic (under N_2)**
α-MnO_2	90 °C	120 °C	65	40	35
β-MnO_2	90 °C	120 °C	50	27	20
γ-MnO_2	90 °C	120 °C	38	15	8
α-MnO_2	120 °C	120 °C	40	15	12
β-MnO_2	120 °C	120 °C	35	Trace	trace
γ-MnO_2	120 °C	120 °C	27	Trace	trace

Table 5.4. Oxidation of diphenylmethane to benzophenone using α-, β-, γ-MnO_2 samples dried at two different temperatures.

Under aerobic conditions, all of the catalysts gave modest to high yields of the oxidation product, whereas under anaerobic conditions α-MnO_2 showed better yield compared to other forms. These results suggest that presence of adsorbed water plays a major role in the oxidation process rather than the morphology of the catalyst. Furthermore, the catalytic loading shown in Table 5.5 was increased from 25 wt% to 500 wt% to reveal a direct correlation of increased yield with increased catalyst, which further supports our claim of adsorbed water involvement in oxidation process.

Table 5.5

Substrate	**25 wt%**	**50 wt%**	**100 wt %**	**500 wt%**
α-MnO_2 (90 °C)	35	50	72	80
β-MnO_2 (90 °C)	20	42	65	74
γ-MnO_2 (90 °C)	8	38	65	78

In summary, α-MnO_2 due to its higher adsorbed water content plays a significant role in the oxidation of diphenylmethane to benzophenone. Whereas surface areas are not that vital for their catalytic activity.

CHAPTER VI

CONCLUSIONS

In the first part of my research differential scanning calorimetry (DSC) was used to monitor the curing behavior and to optimize the conditions for curing epoxy composites. Diglycidyl ether of bisphenol-A type Epon 828 with two different isophoranediamine (IPDA) and 4,4'-diamino-3,3'-dimethyldicyclohexylmethane (DMD) curing agents were used to study the curing behavior. Results suggested that PHR calculated stoichiometric amounts of curing agents should be used to improve properties of the epoxy composites. DSC thermograms showed that the presence of excess amounts of curing agents will reduce the properties of the resulting composites, by acting as a plasticizer. These results helped in the optimization of curing conditions for the preparation of epoxy composites in the second part of my research. DSC thermograms showed an appearance of a second peak at higher temperature regime with an excess of epoxy.

In the second part of my research work we tried to develop an epoxy nanocomposite with the better dispersion of SWNTs as filler material to improve thermal, mechanical and barrier properties. Epoxy/SWNT nanocomposites with a nanotube loading ranging from 0.001-0.01wt.% were prepared and their thermal and mechanical properties were studied. For better dispersion of SWNTs, solvent choice plays a significant role. Results suggested that a better dispersion of SWNTs in the epoxy matrix is important to improve the properties of the epoxy composite. Herein, we reported using a well-established technique, near-infrared fluorescence, in a novel way to evaluate the relatively quality of dispersion in both the solvent and epoxy system, allowing us to maximize the separation of SWNTs into individuals while minimizing damage to the tubes through the ultrasonication processing. Residual solvent content determined by TGA showed complete absence of DMF and little (< 5%) of NMP solvent in the epoxy matrices. DMA results suggested that an increase in storage modulus was observed at very low loadings (0.001-0.01 wt.%) of SWNTs. Contact angle measurements suggested that the hydrophobicity is higher in epoxy nanocomposites compared to plain epoxy composite.

In the third part of my research we synthesized different crystalline forms of MnO_2 such as α-, β-, and γ-MnO_2 by hydrothermal method, to determine catalytic activity assessed in the diphenylmethane to benzophenone oxidation. The role of surface morphology, crystal structure, surface area and water content of the samples were determined. Results showed the amount of adsorbed water had a closer correlation with the catalytic activity of these catalysts.

REFERENCES

(1) Yang, W.; Peters, J. I.; Williams, R. O. *Int J Pharmaceut* **2008**, *356*, 239.

(2) Thostenson, E. T.; Li, C. Y.; Chou, T. W. *Compos Sci Technol* **2005**, *65*, 491.

(3) Hussain, F.; Hojjati, M.; Okamoto, M.; Gorga, R. E. *J Compos Mater* **2006**, *40*, 1511.

(4) Maity, T.; Samanta, B. C.; Dalai, S.; Banthia, A. K. *Mat Sci Eng a-Struct* **2007**, *464*, 38.

(5) Xu, K.; Chen, M. C.; Zhang, K.; Hu, J. W. *Polymer* **2004**, *45*, 1133.

(6) Ray, S. S.; Okamoto, M. *Prog Polym Sci* **2003**, *28*, 1539.

(7) Kurokawa, Y.; Yasuda, H.; Oya, A. *J Mater Sci Lett* **1996**, *15*, 1481.

(8) Furuichi, N.; Kurokawa, Y.; Fujita, K.; Oya, A.; Yasuda, H.; Kiso, M. *J Mater Sci* **1996**, *31*, 4307.

(9) Jeon, H. G.; Jung, H. T.; Lee, S. W.; Hudson, S. D. *Polym Bull* **1998**, *41*, 107.

(10) Privalko, V. P.; Sukhorukov, D. I.; Privalko, E. G.; Walter, R.; Friedrich, K.; Calleja, F. J. B. *J Appl Polym Sci* **1999**, *73*, 1041.

(11) Zax, D. B.; Yang, D. K.; Santos, R. A.; Hegemann, H.; Giannelis, E. P.; Manias, E. *J Chem Phys* **2000**, *112*, 2945.

(12) Kato, C.; Kuroda, K.; Takahara, H. *Clay Miner* **1981**, *29*, 294.

(13) Gao, D. Y.; Heimann, R. B.; Williams, M. C.; Wardhaugh, L. T.; Muhammad, M. *J Mater Sci* **1999**, *34*, 1543.

(14) Chen, G. H.; Chen, X. Q.; Lin, Z. Y.; Ye, W.; Yao, K. D. *J Mater Sci Lett* **1999**, *18*, 1761.

(15) Tabtiang, A.; Lumlong, S.; Venables, R. A. *Eur Polym J* **2000**, *36*, 2559.

(16) Chen, T. K.; Tien, Y. I.; Wei, K. H. *J Polym Sci Pol Chem* **1999**, *37*, 2225.

(17) Yao, K. J.; Song, M.; Hourston, D. J.; Luo, D. Z. *Polymer* **2002**, *43*, 1017.

(18) Dabrowski, F.; Bourbigot, S.; Delobel, R.; Le Bras, M. *Eur Polym J* **2000**, *36*, 273.

(19) Nair, S. V.; Goettler, L. A.; Lysek, B. A. *Polym Eng Sci* **2002**, *42*, 1872.

(20) Lan, T.; Pinnavaia, T. J. *Chem Mater* **1994**, *6*, 2216.

(21) Lan, T.; Kaviratna, P. D.; Pinnavaia, T. J. *Abstr Pap Am Chem S* **1994**, *208*, 284.

(22) Wang, M. S.; Pinnavaia, T. J. *Chem Mater* **1994**, *6*, 468.

(23) Luo, J. J.; Daniel, I. M. *Compos Sci Technol* **2003**, *63*, 1607.

(24) Schmidt, D.; Shah, D.; Giannelis, E. P. *Curr Opin Solid St M* **2002**, *6*, 205.

(25) LeBaron, P. C.; Wang, Z.; Pinnavaia, T. J. *Appl Clay Sci* **1999**, *15*, 11.

(26) Bastola, K. P. 2012, *Preparation and characterization of perfluorooctane sulfonate-intercalated single-walled carbon nanotube ropes and clay-composites* Ph.D thesis, Oklahoma State University.

(27) Kim, H.; Abdala, A. A.; Macosko, C. W. *Macromolecules* **2010**, *43*, 6515.

(28) Ojha, L. R. 2012, *Tailoring of polymer-nanomaterial interactions* Ph.D thesis, Oklahoma State University.

(29) Kannan, R. Y.; Salacinski, H. J.; Butler, P. E.; Seifalian, A. M. *Accounts Chem Res* **2005**, *38*, 879.

(30) Zou, H.; Wu, S. S.; Shen, J. *Chem Rev* **2008**, *108*, 3893.

(31) Lageshetty, S. K. 2009, *Characterization of the thermal and physical properties of nanocomposites of DGEBA epoxy/TiO2 nanoparticles: Investigation of the interactions between nanoparticles and polymer chains* M.S. thesis, Lamar University.

(32) Baughman, R. H.; Zakhidov, A. A.; de Heer, W. A. *Science* **2002**, *297*, 787.

(33) Iijima, S. *Nature* **1991**, *354*, 56.

(34) Ajayan, P. M.; Zhou, O. Z. *Top Appl Phys* **2001**, *80*, 391.

(35) Iijima, S.; Ichihashi, T. *Nature* **1993**, *364*, 737.

(36) Journet, C.; Maser, W. K.; Bernier, P.; Loiseau, A.; delaChapelle, M. L.; Lefrant, S.; Deniard, P.; Lee, R.; Fischer, J. E. *Nature* **1997**, *388*, 756.

(37) Cassell, A. M.; Raymakers, J. A.; Kong, J.; Dai, H. J. *J Phys Chem B* **1999**, *103*, 6484.

(38) Dai, H. J. *Accounts Chem Res* **2002**, *35*, 1035.

(39) Thess, A.; Lee, R.; Nikolaev, P.; Dai, H. J.; Petit, P.; Robert, J.; Xu, C. H.; Lee, Y. H.; Kim, S. G.; Rinzler, A. G.; Colbert, D. T.; Scuseria, G. E.; Tomanek, D.; Fischer, J. E.; Smalley, R. E. *Science* **1996**, *273*, 483.

(40) Alvarez, W. E.; Kitiyanan, B.; Borgna, A.; Resasco, D. E. *Carbon* **2001**, *39*, 547.

(41) Kitiyanan, B.; Alvarez, W. E.; Harwell, J. H.; Resasco, D. E. *Chem Phys Lett* **2000**, *317*, 497.

(42) Odom, T. W.; Huang, J. L.; Kim, P.; Lieber, C. M. *Nature* **1998**, *391*, 62.

(43) Bachilo, S. M.; Strano, M. S.; Kittrell, C.; Hauge, R. H.; Smalley, R. E.; Weisman, R. B. *Science* **2002**, *298*, 2361.

(44) Weisman, R. B.; Bachilo, S. M.; Tsyboulski, D. *Appl Phys a-Mater* **2004**, *78*, 1111.

(45) Lu, M.; Lau, K. T.; Qi, J. Q.; Zhao, D. D.; Wang, Z.; Li, H. L. *J Mater Sci* **2005**, *40*, 3545.

(46) Lau, K. T.; Lu, M.; Lam, C. K.; Cheung, H. Y.; Sheng, F. L.; Li, H. L. *Compos Sci Technol* **2005**, *65*, 719.

(47) Khare, K. S.; Khare, R. *J Phys Chem B* **2013**, *117*, 7444.

(48) Chen, J.; Hamon, M. A.; Hu, H.; Chen, Y.; Rao, A. M.; Eklund, P. C.; Haddon, R. C. *Science* **1998**, *282*, 95.

(49) Margrave, J. L.; Mickelson, E. T.; Chiang, I. W.; Zimmerman, J. L.; Boul, P. J.; Lozano, J.; Liu, J.; Smalley, R. E.; Hauge, R. H. *Abstr Pap Am Chem S* **1999**, *218*, U599.

(50) Mickelson, E. T.; Chiang, I. W.; Zimmerman, J. L.; Boul, P. J.; Lozano, J.; Liu, J.; Smalley, R. E.; Hauge, R. H.; Margrave, J. L. *J Phys Chem B* **1999**, *103*, 4318.

(51) Liu, J.; Rinzler, A. G.; Dai, H. J.; Hafner, J. H.; Bradley, R. K.; Boul, P. J.; Lu, A.; Iverson, T.; Shelimov, K.; Huffman, C. B.; Rodriguez-Macias, F.; Shon, Y. S.; Lee, T. R.; Colbert, D. T.; Smalley, R. E. *Science* **1998**, *280*, 1253.

(52) Park, J. H.; Alegaonkar, P. S.; Jeon, S. Y.; Yoo, J. B. *Compos Sci Technol* **2008**, *68*, 753.

(53) Muzart, J. *Tetrahedron Lett* **1987**, *28*, 2133.

(54) Nammalwar, B.; Fortenberry, C.; Bunce, R. A.; Lageshetty, S. K.; Ausman, K. D. *Tetrahedron Lett* **2013**, *54*, 2010.

(55) Thackeray, M. M. *Prog Solid State Chem* **1997**, *25*, 1.

(56) Rao, C. N. R.; Vivekchand, S. R. C.; Biswas, K.; Govindaraj, A. *Dalton T* **2007**, 3728.

(57) Wang, X.; Li, Y. D. *J Am Chem Soc* **2002**, *124*, 2880.

(58) Khan, Y.; Durrani, S. K.; Mehmood, M.; Khan, M. R. *J Mater Res* **2011**, *26*, 2268.

(59) Sui, N.; Duan, Y. Z.; Jiao, X. L.; Chen, D. R. *J Phys Chem C* **2009**, *113*, 8560.

(60) Truong, T. T.; Liu, Y. Z.; Ren, Y.; Trahey, L.; Sun, Y. G. *Acs Nano* **2012**, *6*, 8067.

(61) Cheng, F. Y.; Zhao, J. Z.; Song, W.; Li, C. S.; Ma, H.; Chen, J.; Shen, P. W. *Inorg Chem* **2006**, *45*, 2038.

(62) Boppana, V. B.; Jiao, F. *Chem Commun* **2011**, *47*, 8973.

(63) Moniruzzaman, M.; Du, F.; Romero, N.; Winey, K. I. *Polymer* **2006**, *47*, 293.

(64) Wang, X.; Li, Y. *J Am Chem Soc* **2002**, *124*, 2880.

(65) Khan, Y.; Durrani, S. K.; Mehmood, M.; Khan, M. R. *J Mater Res* **2011**, *26*, 2268.

(66) Maity, T.; Samanta, B. C.; Dalai, S.; Banthia, A. K. *Mater Sci Eng A* **2007**, *464*, 38.

(67) Juncosa, E. C. 2008. *Adsorption properties of synthetic iron oxides* M.S. thesis, Lulea University of Technology.

(68) Suave, J.; Coelho, L. A. F.; Amico, S. C.; Pezzin, S. H. *Mat Sci Eng a-Struct* **2009**, *509*, 57.

(69) Moniruzzaman, M.; Du, F. M.; Romero, N.; Winey, K. I. *Polymer* **2006**, *47*, 293.

(70) Penumadu, D.; Dutta, A.; Pharr, G. M.; Files, B. *J Mater Res* **2003**, *18*, 1849.

(71) Ausman, K. D.; Piner, R.; Lourie, O.; Ruoff, R. S.; Korobov, M. *J Phys Chem B* **2000**, *104*, 8911.

(72) Nayak, P. K.; Munichandraiah, N. *J Solid State Electr* **2012**, *16*, 2739.

VITA

SATHISH KUMAR LAGESHETTY

Candidate for the Degree of

Doctor of Philosophy

Thesis: (A) EPOXY CURING (B) CHARACTERIZATION OF EPOXY/SWNT NANOCOMPOSITES & (C) MnO_2 NANOSTRUCTURES FOR CATALYSIS

Major Field: Chemistry

Biographical:

Education:

Completed the requirements for the Doctor of Philosophy in Chemistry at Oklahoma State University, Stillwater, Oklahoma in May, 2015.

Completed the requirements for the Master of Science in Chemistry at Lamar University, Beaumont, Texas in 2009.

Completed the requirements for the Bachelor of Science in Pharmacy at Osmania University, Hyderabad, Telangana/India in 2005.

Professional Memberships: American Chemical Society